ELSEVIER

Progress in Quantum Electronics 32 (2008) 121–158

Progress in Quantum Electronics

www.elsevier.com/locate/pquantelec

Review

Wavelength-versatile visible and UV sources based on crystalline Raman lasers

H.M. Pask*, P. Dekker, R.P. Mildren, D.J. Spence, J.A. Piper

MQ Photonics Research Centre, Department of Physics, Macquarie University, Sydney, NSW 2109, Australia

Abstract

By combining stimulated Raman scattering and sum-frequency generation within a single laser system, indeed often within a single resonator, it is possible to achieve frequency conversion over a wide range of output wavelengths, that are useful for a number of applications. This paper reviews the concepts, principles of operation and performance characteristics of visible and ultraviolet (UV) laser systems based on these two nonlinear processes. The systems we review include fixed-wavelength operation in the yellow–orange spectral region (pulsed and continuous wave—CW), discretely tunable pulsed sources operating across the green–red spectral region and discretely tunable UV sources spanning the entire UV-B region.
© 2008 Elsevier Ltd. All rights reserved.

PACS: 42.55.Ye; 42.72

Keywords: Raman lasers; Visible lasers; UV lasers; Solid-state lasers

Contents

*Corresponding author.
E-mail address: hpask@ics.mq.edu.au (H.M. Pask).

0079-6727/$ - see front matter © 2008 Elsevier Ltd. All rights reserved.
doi:10.1016/j.pquantelec.2008.09.001

1. Introduction

An expanding range of important applications in biomedicine, defence and industry underpins intensive ongoing interest in development of new all-solid-state (i.e. semiconductor diode-pumped) visible and ultraviolet (UV) laser sources. Many applications established using older-generation gas lasers and lamp-pumped solid-state lasers are now benefiting from the high efficiency, versatility, compact size, reliability and low cost of the new-generations of all-solid-state lasers, which are also stimulating many new applications in diverse fields.

In this introduction we first summarise key application areas for VIS/UV all-solid-state lasers, with reference to specific source requirements in each area. We then outline the various approaches for the development of VIS/UV all-solid-state lasers that have been explored over the past several years, with emphasis on the most promising contemporary developments. Finally we introduce the key concepts of VIS/UV laser development based on crystalline Raman lasers, which employ simultaneous stimulated Raman scattering (SRS) and second-harmonic generation (SHG) of the fundamental wavelengths of conventional diode-pumped solid-state lasers to generate multiple, selectable wavelengths spanning the visible and UV.

1.1. Applications for VIS/UV all-solid-state lasers

Although some high-profile applications, notably laser guide stars and large-scale laser projection display, require high powers (tens of watts) in the visible (589 nm in the first case

and RGB in the second), the great majority of applications require quite moderate powers, ranging from only a few milliwatts to a few watts. For these latter, compact size, efficiency, reliability, versatility and cost are critical practical requirements.

Biomedical diagnostics based on light scattering and fluorescence detection usually need quite low powers, and often quite relaxed spectral bandwidth specifications, but good beam quality is almost always important, as is the capability for generating a range of wavelengths across the visible and UV spectrum. Specific applications include fluorescence imaging and scanning (e.g. capillary-gel readers for DNA sequencing), and confocal microscopy. Flow cytometry additionally requires very-low amplitude noise and high beam-pointing stability. There are a number of applications in *therapeutic medicine* requiring VIS/UV output powers in the 1–3 W range. Perhaps the most important of these are in ophthalmology, where access to several visible wavelengths from green to red is desirable to enable the light energy to interact with different pigments in the eye. Similar requirements for wavelength versatility apply in dermatology, where selective interactions with melanin, haemoglobin or collagen may be necessary for different procedures.

Defence and security applications of VIS/UV lasers generally centre on remote sensing in a variety of forms, for example, laser bathymetry or underwater detection requiring different blue–green–yellow wavelengths for different water conditions, biological detection in the UV and counter-measures related to optical detectors.

Laser projection display for advertising, entertainment, and large-scale TV or cinema has motivated a number of recent developments of high-power solid-state lasers with RGB outputs (true colour projection may require up to five wavelengths across the visible). Recent developments of small-scale laser projection systems, which might be incorporated in mobile phones, for example, have stimulated interest in the low-power (~10 mW) miniature all-solid-state lasers with high beam quality and a variety of accessible wavelengths. The broad field of *reprographics* is one where the cost, size and electrical efficiency of all-solid-state VIS/UV lasers make them very attractive alternatives to ion lasers, and a variety of *industrial sensing* applications demand a range of low-power lasers with specific wavelengths spanning the spectrum from deep UV to the red.

1.2. Approaches to the development of all-solid-state VIS/UV lasers

VIS–UV lasers based on SHG or sum-frequency generation (SFG) of diode-pumped Nd^{3+} crystalline lasers are ubiquitous. To the standard 532, 355 and 266 nm wavelengths of frequency-doubled, -tripled and -quadrupled (1064 nm) Nd:YAG and vanadate lasers have been added the 473 nm output from frequency doubling of the 946 nm transition, 556 nm from frequency doubling of the 1112 nm transition [1], and even 671 and 336 nm from frequency doubling and quadrupling of the 1342 nm transition (generally using vanadate hosts) [2,3]. SFG of the 1064 and 1320 nm outputs of separate high-power Nd:YAG lasers has been used to generate powers up to 50 W at 589 nm for laser guide stars [4], and in much smaller packages for more general use, continuous wave (CW) powers ~1 W can be obtained by intracavity SFG of the 1064 and 1342 nm lines oscillating simultaneously in a Nd:YVO_4 laser at diode-yellow conversion efficiencies better than 10% [5]. While direct SHG/SFG of Nd^{3+} lasers is perhaps the simplest approach for providing VIS/UV sources, this does suffer from the disadvantage that effectively only one visible output wavelength can be delivered at any time, and there is comparatively limited choice in wavelength.

A number of different solid-state and fibre laser schemes for generating VIS/UV output have been explored in some detail over the past decade. Up-conversion lasers based on Er^{3+} in fluoride crystal hosts have most recently generated up to 0.5 W in the green (552 nm) with 30% slope efficiency [6], though these require high-brightness pumps and there is limited scope for extension to other dopants in practical devices. Up-conversion lasers based on Pr^{3+}-, Er^{3+}- or Tm^{3+}-doped fluoride (ZBLAN) fibres have been subject to quite extensive development, and can deliver CW powers of hundreds of milliwatts over a range of visible wavelengths, but they suffer from practical difficulties, particularly fragility of the fibres [7]. More recently there have been notable advances in the development of CW yellow sources based on external frequency doubling of the polarised outputs of either narrow-band Yb-fibre lasers [8] or Raman fibre lasers pumped by Yb-fibre lasers [9]. In the latter case, CW powers up to 3 W have been demonstrated in the yellow at overall diode-visible conversion efficiencies of several percent. The very broad gain bandwidths of Yb- and Er-doped fibre lasers show promise of a broad range of available visible wavelengths that might be generated using this approach, though the systems remain quite complex and miniaturisation is challenging.

One of the most significant recent developments of visible all-solid-state lasers, and arguably the most advanced commercially (apart from frequency-doubled Nd lasers), is represented by the family of (frequency doubled) optically pumped semiconductor lasers (VECSELs) [10]. These devices use vertically stacked InGaAs multiple-quantum-well thin disks with integral spacer layers and Bragg rear mirrors, and vertical-external cavities incorporating nonlinear frequency doublers. CW output powers >7 W have been obtained over a range of wavelengths from 460 to 577 nm, and as much as 64 W at 532 nm [11]. Any wavelength between 460 and 580 nm can be generated in principle, though the semiconductor chip must be purpose designed for a given operating wavelength. Thermal effects in the chip at high pump powers also pose some problems for achieving good beam quality at high (multi-watt) powers, though multichip configurations have been successful in alleviating these.

A new generation of all-solid-state VIS–UV lasers may also be stimulated by the availability of high-brightness blue diodes based on GaN semiconductor technology for the direct pumping of solid-state laser media. For example, GaN-diode-pumped Pr:YLF lasers giving CW outputs in the green and red with up to 40% percent slope efficiency [12] and frequency doubling to the UV (320 nm) [13] have already been reported.

1.3. VIS–UV sources based on crystalline Raman lasers

An alternative generic approach to the development of all-solid-state visible and UV laser sources is based on simultaneous SRS and SHG/SFG of fundamental wavelengths of otherwise "conventional" diode-pumped crystalline solid-state lasers. Combinations of fundamental wavelengths of Nd^{3+} lasers, with various Stokes orders and different Stokes shifts of a range of practical Raman crystals plus the capability of achieving simultaneous SHG or SFG of different Stokes orders provide for an extensive range of accessible wavelengths with surprisingly high optical conversion efficiencies (diode to visible $>10\%$). Moreover, the cascading effect of SRS in combination with intracavity SHG/SFG permits a high degree of flexibility in selecting the output wavelength from a single device, including the unique option of switching from one visible wavelength to another. This approach also takes advantage of the enormous investments already made in the

engineering of diode-pumped solid-state lasers, including miniaturisation, and the existence of a number of excellent self-Raman laser crystals.

Although the first demonstration of a crystalline Raman laser (using a lamp-pumped solid-state laser for the fundamental) was reported nearly 30 years ago [14], there have been substantial advances in the past decade coincident with the increasing availability of high-quality Raman crystal materials and accelerated development of high-power-diode-pumped solid-state lasers. A number or reviews on various aspects of crystalline Raman lasers have been completed [15–18]. The most recent by Piper and Pask [18], in 2007, focused on advances in the previous 5 years. However, there have been significant advances of all-solid-state VIS–UV sources based on crystalline Raman lasers only in the past 2 years, notably the first reports of efficient CW visible sources and demonstration of multi-wavelength pulsed UV sources covering critical application areas.

There follows a more extended introduction to the nonlinear processes of SRS and sum-frequency generation in the context of combining them to generate VIS–UV outputs from all-solid-state lasers, discussion of key properties of crystalline Raman media and alternative Raman laser configurations (Section 2). Since SRS and SFG/SHG can each be carried out either intracavity or extracavity, there is a range of configurations that can be employed to obtain the wavelengths described above. In the following sections, work in the field has been reviewed broadly according to the configuration used. Extracavity-doubled Raman lasers are reviewed in Section 3, intracavity-doubled intracavity Raman lasers in Sections 4 and 5, external-resonator Raman lasers in Section 6 and intracavity-doubled external-resonator Raman lasers in Section 7.

2. Background to frequency conversion using SRS and SFG

In this section, we briefly review the two nonlinear processes of SRS and SFG in the context of combining them in a Raman-laser-based system. We will also detail the key design considerations and discuss the potential of this approach for accessing a wide range of wavelengths in the visible and UV.

Both SRS and SFG rely on the nonlinear polarisation P induced in a material by an electric field E, written as

$$P(E) = \kappa_0 E + \chi^{(2)}E^2 + \chi^{(3)}E^3 + \cdots \quad (1)$$

in which P and E are vectors, and $\chi^{(2)}$ and $\chi^{(3)}$ are the second and third-order nonlinear polarisability tensors, giving rise to SFG/SHG and SRS, respectively. The polarisability tensors are a property of the material. All materials exhibit odd-order polarisabilities to some degree but only materials that lack inversion symmetry display even-order polarisabilities.

2.1. Key design considerations for conversion via SRS

Raman scattering is a $\chi^{(3)}$, nonlinear inelastic process in which a photon interacts with a Raman-active medium, resulting in a photon of lower energy (Stokes photon) and a phonon—a quanta of vibration in the material. Energy and momentum conservation requirements apply: $\omega_P = \omega_S + \omega_R$ and $k_P = k_S + k_R$, where ω and k are the angular frequency and wavevector of the excitations, and the subscripts P, S, and R refer to the pump photon, the Stokes photon and the phonon, respectively. Despite the requirement

for momentum conservation, the lack of phonon dispersion $d\omega_R/dk_R \approx 0$ allows a wide range of momentum values to be taken up by the phonon, and so the spontaneous Stokes photons may be emitted at any angle to the incident pump photon. For a full description of the physics of SRS, the reader is referred to a review paper by Penzkofer et al. [19], or an introductory text by Boyd [20].

SRS is well established as a means of frequency conversion [15–18] and can be extremely efficient. Indeed conversion efficiencies as high as 95% have been reported [21], close to the ultimate efficiency determined by the ratio of Stokes to fundamental photon energies. Stimulated amplification occurs dominantly for a Stokes wave propagating so that overlap with the pump wave is maintained. This means that a fundamental beam will predominantly generate a co-propagating Stokes beam (forward SRS), with the Stokes intensity I_S growing exponentially as it propagates according to

$$I_S(l) = I_S(0)\exp(I_P g_R l) \tag{2}$$

Here the small-signal gain is determined by the pump intensity I_P, the Raman gain coefficient g_R and the crystal length l. Pump depletion will of course eventually diminish the gain. If the first-Stokes wave becomes sufficiently intense, it can itself become Stokes shifted, generating a "second-Stokes" beam. Continuing this process, the so-called "cascaded" SRS can easily generate three or four Stokes orders, particularly in external-cavity or intracavity Raman lasers for which the cavity has a high Q for all of the generated wavelengths. The intensity of the ith Stokes order thus depends on the conversion rate from the $(i-1)$th Stokes order (proportional to $g_R I_i I_{i-1}$) and loss rate to the $(i+1)$th order (proportional to $g_R I_i I_{i+1}$). Cascading is an important basis for the multiple-wavelength and wavelength-selectable Raman lasers reviewed below.

2.1.1. Raman configurations

There are numerous design options for lasers employing SRS that can be used to tailor Raman laser characteristics and performance. Three basic configurations are shown schematically in Fig. 1. The *Raman generator* is the simplest, with a pump beam (often focused or telescoped) into a Raman crystal to generate a Stokes beam. Typically used with short pulse (picosecond—ps) lasers, this process has yielded efficiencies as high as 95% [21], and is capable of generating a large number of Stokes and anti-Stokes lines. For pump pulses that are longer than the transit time through the Raman crystal, it is beneficial to place the Raman crystal inside a cavity that resonates the Stokes field. This *external-resonator Raman laser* allows multiple-pass amplification of the Stokes field, which is coupled out through the partially reflecting output mirror. Often the output mirror is made reflecting at the pump wavelength so that the pump beam makes a double-pass through the crystal. The *intracavity Raman laser* combines a Raman medium as well as the laser medium inside a single cavity so that the fundamental and Stokes fields are both resonated within the cavity. Incorporating the Raman material inside the laser cavity in this way makes use of high intracavity powers to allow conversion of lasers whose output would be of too low power to convert.

The choice between these three configurations is typically driven by the required output characteristics and the available pump lasers. Raman generators and external-cavity Raman lasers require pump sources with relatively high brightness, but can otherwise be a simple "add-on" to the pump source. On the other hand, intracavity Raman lasers are more complex "stand-alone" systems, but can be pumped by cheap laser diodes with

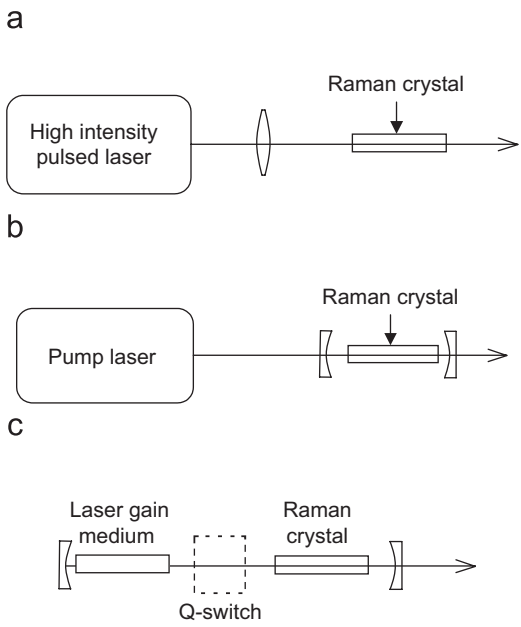

Fig. 1. Schematic diagrams of common Raman laser configurations. (a) Raman generator, (b) external Raman resonator and (c) intracavity Raman laser.

relatively poor beam quality. This paper focuses on external-resonator and intracavity Raman lasers, in which the presence of a resonator plays an important role in shaping the output characteristics of the device. Raman generators are not covered in detail by this review. However, they have been previously reviewed in detail in [16].

2.1.2. *Raman crystal selection*

The choice of Raman crystal rests on a combination of factors, including the target wavelength, Raman gain coefficient, the threshold for optical damage and thermal properties, which determine the extent of thermal lensing. Table 1 shows the properties of some commonly used Raman crystals, including most of those used in the lasers reviewed in this paper.

Raman gain is generally higher in covalent bonded crystals compared to ionic bonded crystals: diamond has a particularly high Raman cross-section, and the tungstates, nitrates and vanadates amongst others also exhibit strong Raman activity. While $Ba(NO_3)_2$ has long been favoured for its high gain, the crystal is easily damaged and is significantly hygroscopic. Many of the recent advances in crystalline Raman lasers have been enabled either by the development of new Raman crystals and/or by identifying the Raman laser potential of well-known crystals that have been traditionally used for other applications. Of particular note are the tungstates, vanadates and diamond.

Tungstate crystals have been widely investigated as Raman media [24,29,30] and fall into two categories. Of the double-metal tungstates, $KGd(WO_4)_2$ (KGW) has been widely deployed, owing to its combination of ease of handling, high damage threshold, and good thermal conductivity. The tetragonal tungstates which include $PbWO_4$, $SrWO_4$ and $BaWO_4$ amongst others, are also becoming more widely used for Raman shifting, and of

Table 1
Important optical and thermal properties for selected Raman crystals [16,17,22–28]

	Raman shift (cm^{-1})	Gain coeff. at 1064 nm (cm/GW)	Gain coeff. at 532 nm (cm/GW)	Damage threshold (GW/cm^2)	Thermal conductivity ($W\,m^{-1}\,K^{-1}$)	Thermo-optic coeff. at 1064 nm (K^{-1}) $\times 10^{-6}$
KGW	768 901	4.4 3.5	11.8	10	2.6 [100] 3.8 [010] 3.4 [001]	−0.8 (p[gg]p) −5.5 (p[mm]p)
$Ba(NO_3)_2$	1047	11	47	0.4	1.17	−20
$BaWO_4$	926	8.5	40	–	3	–
$GdVO_4$	885	4.5	–	1	5	3
$LiIO_3$	822	4.8	–	0.1	–	−84.9(o) −69.2(e)
KTP	270	–	–	15	2 [100] 3 [010] 3.3 [001]	6.1 (*x*-pol) 8.3 (*y*-pol) 14.5 (*z*-pol)

these, $BaWO_4$ is particularly attractive due to its high Raman gain and narrow linewidth. Notably, the highest Raman conversion efficiency was achieved in this material [21]. Recent work on the development and application of tungstate crystals can be found in [31–33].

While vanadate crystals $GdVO_4$ and YVO_4 have been widely used as Nd laser host materials and in telecoms applications, the potential of these crystals as Raman media was recognised only recently [23]. They have excellent optical properties and provide good Raman gain, and Nd-doped crystals are particularly well suited for use in ''self–Raman'' laser configurations, in which the same crystal is used as both laser and Raman medium [34,35].

Finally we note very recent work in the use of synthetic diamond, grown by chemical vapour deposition, for Raman laser applications. Diamond has a large Raman shift, 1332 cm^{-1}, and the Raman gain coefficient for single-crystal diamond and a pump wavelength of 1064 nm was reported to be 12.5 cm/GW [36]. The same group reported several Stokes and anti-Stokes lines in a 0.67 mm thick single crystal sample [36] and previously in a polycrystalline sample [37], when pumped with 532 and 1064 nm picosecond lasers. A pulsed, diode-pumped diamond Raman microchip laser was also reported in [38]. The large band gap of diamond and the high thermal conductivity make it very promising for Raman conversion at wavelengths as short as 230 nm and for scaling Raman laser output to very high average powers.

2.1.3. Raman resonator design

The key to achieve efficient frequency conversion through SRS is optimising the resonator design, including mirror reflectivity and curvature, resonator length and placement of components. Generally, increasing the single-pass gain is desirable. It follows from Eq. (2) that this can be done by increasing the crystal length, decreasing the size of the beams in the crystal or choosing a crystal with a higher Raman gain coefficient. Other constraints include keeping intensities sufficiently low so as to avoid unwanted higher-order Stokes orders and competing nonlinear effects such as self-focussing, and avoiding optical damage to the crystal and any optical coatings.

As will be seen in many of the following sections, the coating characteristics of resonator mirrors are particularly important design parameters. Specific requirements vary according to the resonator configuration and whether intracavity SHG is employed. Typically the coatings are designed to admit a pump beam and resonate one or more of the fundamental and/or Stokes waves. The choice of mirror reflectivity for each Stokes order determines how "cascading" of the SRS process proceeds and where it terminates. For Q-switched external-resonator Raman lasers emitting in the visible, output coupler reflectivity is typically in the range 10–50%, while for intracavity-doubled Raman lasers, broadband high reflectors can be used since output coupling is by way of SFG/SHG. For CW lasers, very high reflectivity mirrors are required to minimise resonator losses. In many cases, the design requirements on cavity mirrors are demanding. Custom-designed coatings are often required, and indeed the availability of suitable coatings can place a limit on the performance of specific laser systems.

Of critical importance are the resonator mirror curvatures and the layout of components, as these can be used to alter the mode size in each of the intracavity crystals. The mode size in the Raman crystal influences the conversion efficiency to the selected Stokes order and also loss to higher Stokes orders. When intracavity doubling is employed, the mode size in the doubling crystal must also be considered. The optimization of mode sizes is achieved through a careful choice of mirror curvature, cavity length and placement of crystals.

Thermal lensing in Raman crystals, stemming from the inelastic nature of the scattering process, can impact markedly on resonator design, particularly in Raman lasers designed for high average power and/or high repetition rate operation, and must be taken into account. Thermal lensing issues in crystalline Raman lasers are treated in detail in Ref. [15]. Generally, for an end-pumped laser, the effective focal length of the thermal lens (arising from the thermo-optic effect) can be estimated using

$$\frac{1}{f_{\text{thermal}}} = \left(\frac{\mathrm{d}n}{\mathrm{d}T}\right)\frac{1}{K_C}\frac{P_S}{\pi r_S^2}\left(\frac{\omega_P}{\omega_S} - 1\right) \tag{3}$$

where the thermal lens is seen to scale as the average power at the first-Stokes line (P_S) and the thermo-optic coefficient ($\mathrm{d}n/\mathrm{d}T$), and inversely as the square of the Stokes mode radius (r_S) and the thermal conductivity of the crystal (K_C).

2.2. Key design considerations for conversion via SHG and SFG

SFG is a very well-known $\chi^{(2)}$ nonlinear process of which SHG is a special case, and background texts include those by Boyd [20] and Davis [39]. For a detailed description of phase-matching properties of the many crystals used for SFG/SHG, as well as many examples in which each has been used, the reader is referred to the book by Dmitriev et al. [40].

In practical terms, SFG crystals are usually selected on whether phase matching can be achieved for the desired wavelength without deleterious absorption of the generated light (in particular for UV wavelengths). For efficient conversion, d_{eff} should be high, crystal length long and the angular and temperature acceptance bandwidths large such that the phase mismatch $\Delta k \sim 0$. It is also worth noting that birefringent walk-off, in which different polarisations in a birefringent crystal become spatially separated, thereby reducing the overlap of the co-propagating beams as they propagate, limits the practical crystal length

that may be used. "Non-critical" phase matching alleviates this limitation by phase matching along an optical axis of the crystal, avoiding walk-off, and also reduces sensitivity to angular misalignment. Other parameters that also need consideration in terms of practicality include optical damage threshold and hygroscopy. SFG/SHG may be carried out extracavity or intracavity. For pulsed laser sources with substantial (kW) peak powers, external doubling generally proceeds efficiently. For lower power laser sources, and particularly CW lasers, it is necessary to use intracavity doubling, where the doubling crystal is placed inside the laser resonator.

Table 2 provides a starting point for comparing the various crystals that are most useful for SHG to the visible and UV [41]. LBO and KTP are often favoured for sum-frequency mixing of wavelengths around 1064 nm. KTP has a relatively high d_{eff}, but exhibits substantial walk-off. LBO, on the other hand, has a lower d_{eff}, but can be oriented for non-critical phase matching. $LiIO_3$ and KTP are particularly interesting crystals since they can also be used for Raman scattering [14,42]. For doubling visible wavelengths into the UV region, BBO and KDP are the most commonly used crystals. LBO is also useful, despite a relatively low d_{eff}. BBO has a higher d_{eff} than KDP, but the advantage this brings is traded off against its larger walk-off angle.

Table 2
Comparison of various nonlinear crystals for SFG/SHG to the visible and UV

	LBO	BBO	KTP	$LiIO_3$	KDP
Possible output wavelengths (nm)	>280	>205	500–540 (*XY*-plane) >540 (*XZ*-plane)	>300	>260
Typical properties for SHG of 1176–588 nm					
Phase-matching configuration	Type 1 $\theta = 90°$, $\varphi = 0°$ *XY*-plane 315 K	Type 1 $\theta = 21.5°$, $\varphi = 0°$ *XZ*-plane 300 K	Type 2 $\theta = 69°$, $\varphi = 0°$ *XZ*-plane 300 K	Type 2 $\theta = 27°$, $\varphi = 0°$ *XZ*-plane 300 K	Type 1 $\theta = 42°$, $\varphi = 0°$ *XZ*-plane 300 K
d_{eff} (pm/V)	0.84	2.0	3.5	2.2	0.26
Walk-off (mrad)	0	53	34	69	28
Acceptance angle (mrad cm)	187	1.35	1.89	0.92	2.86
Temp. range (K cm)	7	51	28	78	12
Accept. bandwidth (cm^{-1} cm)	153	56	10.2	16.7	87.5
Typical properties for SHG of 588–294 nm					
Phase-matching configuration	Type 1 $\theta = 90°$, $\varphi = 66°$ *XY*-plane 300 K	Type 1 $\theta = 41.6°$, $\varphi = 0°$ *XZ*-plane 300 K	NA	NA	Type 1 $\theta = 62.4°$, $\varphi = 0°$ *XZ*-plane 300 K
d_{eff} (pm/V)	0.37	1.86			0.41
Walk-off (mrad)	14	83			26
Acceptance angle (mrad cm)	2.53	0.42			1.53
Temp. range (K cm)	4.3	8			3.6
Accept. bandwidth (cm^{-1} cm)	12.4	7.7			15.1

Data taken from SNLO software [41].

2.3. Design potential for multi-wavelength operation and wavelength selectability

SRS can be used either on its own or in combination with SFG/SHG to access a wide variety of output wavelengths in the UV, visible and near-infrared. This is illustrated in Fig. 2, which shows the wavelength regions that can be accessed by the two most commonly used pump wavelengths: 1064 nm from an Nd:YAG laser and its second harmonic at 532 nm. The graphs show the first- and second-Stokes wavelengths as a function of Raman shift, with the vertical axis also showing the wavelengths that can be achieved by SHG of the Stokes lines. For both 1064 and 532 nm pump sources there is particularly good coverage of the yellow–orange spectral region and also the UV region between 270 and 300 nm. Fig. 2 can be used in conjunction with the Raman shifts of a particular crystal (e.g. those in Table 1) to find what wavelengths are accessible. Clearly, by choosing a different pump source, such as a laser using a different Nd host, a 1.3 μm Nd transition or another laser system altogether, a different range of wavelengths can be accessed.

Of particular interest in this paper are lasers in which SRS and SHG/SFG proceed within a single resonator, and it is these systems that give rise to the unique wavelength-selective operation that the authors of this paper think to be particularly interesting and applicable for a diverse range of applications.

Fig. 3 shows schematically how cascaded SRS of a fundamental laser can be combined with SHG and SFG to generate wavelength-selectable output. A resonator is used, which is capable of resonating several optical fields (e.g. the fundamental, first and second Stokes) of the intracavity Raman laser, and a nonlinear crystal is used, which can be easily re-configured to phase match any one of several nonlinear interactions to selectably generate one of several possible visible output wavelengths. Clearly, if the nonlinear crystal is phase matched to double the fundamental at say 1064 nm, SHG of the fundamental proceeds efficiently, and provided the nonlinear coupling coefficient is sufficiently high, no significant first Stokes is generated. If the nonlinear crystal is de-tuned so that there is no SHG of the fundamental, then the first-Stokes optical field builds rapidly and the nonlinear crystal can be tuned to allow either SFG of the fundamental and first-Stokes lines, or SHG

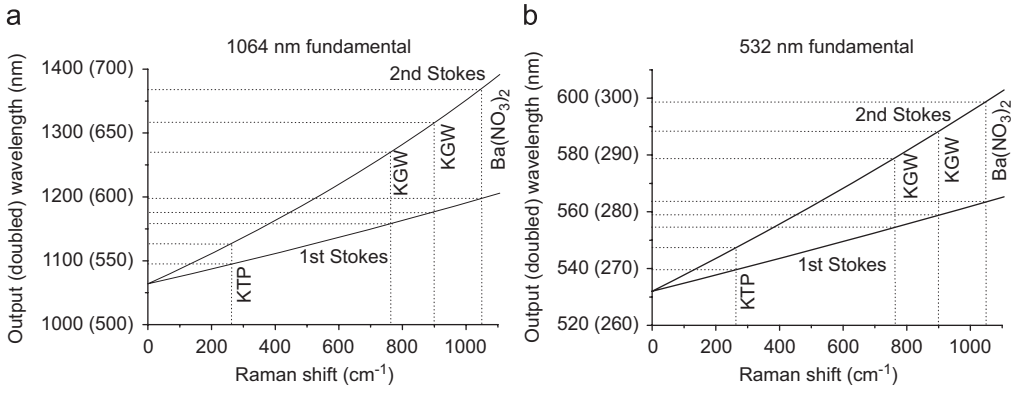

Fig. 2. Raman laser output wavelengths (and doubled wavelengths) are shown as a function of Raman shift using, for pump, wavelengths of (a) 1064 and (b) 532 nm. Discrete wavelengths are indicated for some examples of Raman materials.

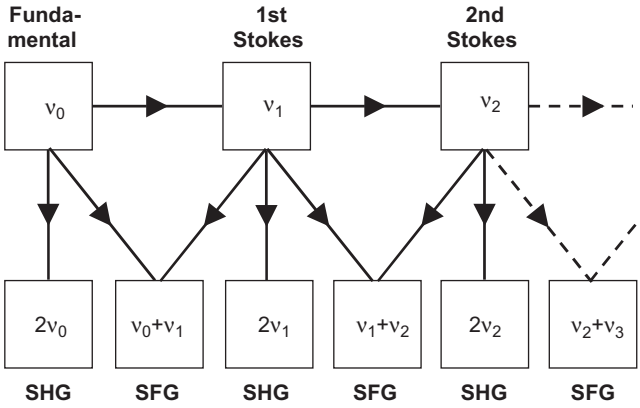

Fig. 3. Schematic diagram showing cascaded SRS of a fundamental laser of frequency v_0 and the resulting selectable output frequencies available via SHG and SFG.

of the first Stokes. Thus by angle or temperature tuning of a suitable intracavity SFG crystal, we can choose to double any of these fields or create a sum-frequency field from adjacent orders. Assuming the resonator mirror reflectivities are sufficiently broad, conversion to second- or even third-Stokes lines can occur, and the nonlinear crystal can be configured to allow sum-frequency mixing of the first and second Stokes, or SHG of the second Stokes.

Examples of how this scheme has been applied to an intracavity Raman laser, thereby generating wavelength-selective output across the green–yellow–red region, can be found in Section 4, while a wavelength-selective UV laser based on applying this scheme to an external-resonator Raman laser pumped at 532 nm is reviewed in Section 7.

3. Extracavity SHG/SFG of Raman lasers

In this section, we consider examples of Raman-based lasers that have been frequency doubled in order to generate visible or UV output at novel wavelengths. To our knowledge, all such sources are pulsed. While extracavity doubling of a laser output is not novel in itself, we include such sources in this paper because a great many wavelengths can be achieved with great simplicity.

Types of Raman lasers that have been extracavity doubled include Raman generators, external-resonator Raman lasers pumped at 532 or 1064 nm, and intracavity Raman lasers that may be intracavity doubled. The frequency-doubling stage typically comprises one or more lenses for optimally focussing into the frequency-doubling crystal. The design considerations for extracavity doubling are covered well in Boyd [20] and Davis [39].

Around 20 papers have reported extracavity doubling of Raman lasers with wavelengths ranging from UV to orange. The performance characteristics of a number of extracavity-doubled Raman laser-based sources are presented in Table 3.

A wide variety of infrared Raman lasers have been doubled into the visible, for applications ranging from guide star to low-power biomedical sources. The highest visible output, 90 mJ at 588 nm, was reported by Murray et al. [43] for guide star applications,

Table 3
Selected visible/UV lasers based on extracavity doubling of Raman laser sources

SH wavelength (nm)	Raman-laser-based source	Raman laser output	SHG crystal	SH output power/ energy (pulse duration, prf)	SHG efficiency (%)	Ref.
10 Lines 262–308	Copper-laser-pumped $Ba(NO_3)_2$ Raman generator	600 mW (539 nm) 300mW (615 nm)	KDP DKDP	1–80 mW (<14 ns, 16 kHz)	13	[46]
281	External resonator Raman laser ($Ba(NO_3)_2$, 532 nm pump)	34 mJ (563 nm)	DKDP	4.2 mJ (11 ns)	32	[44]
289	Intracavity-doubled intracavity Raman laser (Nd:YAG/$LiIO_3$/LBO)	1.4 W (578 nm)	BBO	250 mW (12 ns, 10 kHz)	26	[47]
578	Intracavity Nd:YAG/$LiIO_3$ Raman laser	1.6 W (1156 nm)	LBO	550 mW (30 ns, 4 kHz)	18	[48]
581	300 W QCW-diode-pumped Nd:KGW self-Raman laser	0.1 mJ	LBO	30 μJ (16 ns)	30	[49]
581	300 W side-pumped intracavity Nd:YAG/ $NaBrO_3$ Raman laser	0.4 mJ	LBO	0.15 mJ (5 ns, 47 Hz)	38	[50]
588	5 W-diode-pumped intracavity Raman laser (Nd:YAG/ $CaWO_4$)	480 mW (1178 nm)	LBO	250 mW (10 kHz)	52 (5% wrt diode)	[43]
589	Nd:YLF/ $Ba(NO_3)_2$ flashlamp-pumped Raman laser	250 mJ (1178 nm)	LBO	90 mJ (1.5 ns, 10Hz)	36	[51]
588	1.8 W-diode-pumped intracavity Nd:YVO_4 Raman laser	182 mW (1176 nm)	LBO	3.5 mW (30kHz)	2	[52]
588	1.8 W-diode-pumped intracavity Nd:$GdVO_4$ Raman laser	100 mW (1176 nm)	LBO	3 mW (<19 ns, 10 kHz)	3	[53]
591	300 W QCW-diode-pumped Nd:KGW self-Raman laser	0.8 W (1181 nm)	LBO	0.2 W (2 ns, 2 kHz)	25	[54]
599	300 W side-pumped intracavity Nd:YAG/ $Ba(NO_3)_2$ Raman laser	2.5 mJ (1197 nm)	LBO	0.6 mJ (5 ns, 47Hz)	24	[50]
599	Nd:YAG-pumped $Ba(NO_3)_2$ Raman laser	42 mJ (1197 nm)	LBO	18.5 mJ (~5 ns)	43	[55]
599	Nd:YAG-pumped $Ba(NO_3)_2$ Raman laser	1.3 W (1197 nm)	LBO	0.27 W (4 ns, 4 kHz)	20	[56]
240–598	1 W diode-pumped Nd:LSB/ $Ba(NO_3)_2$ Raman microchip laser	70 mW average 48 kW peak (1196 nm)	LBO BBO KTP	Not given	–	[45]

while the highest UV output, 4.2 mJ at 281 nm, was reported by Ermolenkov et al. [44] for differential lidar remote sensing of tropospheric ozone.

Of particular interest in showing how a diversity of output wavelengths can be generated by extracavity SHG is the recent work by Demidovich et al. [45]. The Raman laser reported was a passively Q-switched microchip laser based on a 1.24-mm-thick Nd:LSB

laser crystal and a 2-mm-thick $Ba(NO_3)_2$ crystal, which generated first-Stokes pulses of duration 48–180 ps and peak power up to 48 kW. The diode-pump power was a modest 1 W. The high peak powers at the Stokes and fundamental wavelengths made it possible to obtain 11 new wavelengths by a combination of SFG and SHG, and the system has the potential to be very compact.

4. Pulsed intracavity Raman lasers with intracavity SHG/SFG

Almost 30 years ago, Ammann [14] reported an intracavity Raman laser based on an arclamp-pumped Q-switched Nd:YALO crystal and an intracavity lithium iodate crystal. $LiIO_3$ has both second- and third-order nonlinearity and was configured to serve both as a Raman medium and as a sum-frequency-mixing crystal. Four laser lines were generated in the yellow to red spectral range (in addition to the second harmonic of the fundamental at 540 nm) by rotating the $LiIO_3$ angle to phase match different combinations of the resonant fundamental, first- and second-Stokes wavelengths. The highest output power of 685 mW was obtained at 592 nm, the second harmonic of the first-Stokes wavelength.

More recently, Mildren et al. [57] and Li et al. [58] used diode-pumped, Q-switched Nd:YAG systems, with separate crystals for the Raman and frequency-mixing processes to achieve high overall conversion efficiencies (diode-yellow ~8%) and visible output powers over 3 W. This arrangement also permits a wider choice of Raman and frequency-mixing materials and therefore output wavelengths. However, the early work by Ammann is very significant in terms of showing the potential for achieving a diversity of output wavelengths from a laser incorporating both SRS and nonlinear frequency mixing. Note that while $LiIO_3$ has a number of practical disadvantages (low damage threshold, hygroscopic), there are other crystals (notably KTP) that can also be used as dual function (Raman/nonlinear mixing) media. KTP has been used as such in an external-resonator Raman laser pumped by a fibre laser [59] as well as in an intracavity Raman laser [42].

Since the early work by Ammann, the vast majority of pulsed intracavity Raman lasers with intracavity SHG/SFG has been focussed on generating fixed-wavelength yellow–orange output, and Section 4.1 focuses on that work. Section 4.2 focuses on systems that are wavelength selectable.

4.1. Fixed-wavelength lasers

4.1.1. Design principles

Fig. 4a depicts the simplest configuration for an intracavity Raman laser with intracavity SHG. The laser crystal is typically doped with Nd and operated at the fundamental transition around 1064 nm, although other laser transitions and active ions can be used. The resonator mirrors are typically coated so as to admit the pump light from a laser diode (when end-pumping is used), and to resonate the fundamental and first-Stokes optical fields. The output coupler also has high transmission in the visible (to couple out the second harmonic). The Q-switch is typically an acousto-optic Q-switch, enabling high peak powers to be achieved at kHz repetition rates. A wide variety of Raman crystals may be used, including those listed in Section 2, while suitable doubling crystals include LBO, BBO, KTP and RTP.

As noted in Section 2, this type of laser involves three optical processes occurring in a single laser resonator, and the key to efficient laser operation is to ensure that the laser

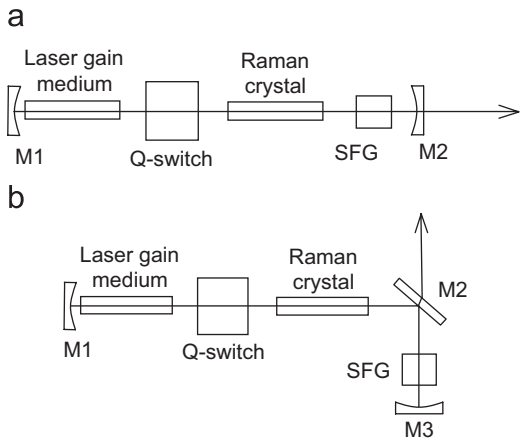

Fig. 4. (a) Linear and (b) folded resonator architectures for pulsed intracavity Raman lasers.

parameters are simultaneously optimised for the fundamental laser generation, conversion to the first Stokes and for frequency doubling of the first Stokes. This is achieved through careful selection of the laser, Raman and doubling crystals, and careful resonator design to optimise the mode sizes in each of these crystals. Importantly, the resonator design must account for thermal effects, which are typically present and frequently strong in the laser and Raman crystals.

The resonator configuration in Fig. 4a is limited in that only the second harmonic generated in one direction is coupled into the output beam. The output generated in the other direction is typically absorbed in the laser crystal, thereby contributing to the thermal load, or transmitted through mirror M1. Therefore it is desirable to design a resonator (such as that shown in Fig. 4b) that enables the visible output generated in both directions to be coupled into a single output beam.

A number of laser, Raman and doubling crystals can be used which provide the dual functions of either laser and Raman media (so-called self-Raman) or Raman and doubling media. This gives rise to great potential for miniaturisation.

4.1.2. Review of selected results

The performance of selected Q-switched intracavity-doubled Raman lasers is summarised chronologically in Table 4. This diverse group of lasers has employed diode end-pumping, side-pumping (by arc lamps or laser diodes), four different Nd laser materials, seven different Raman media and three different doubling crystals. Clearly there is much scope for optimisation to achieve desired output characteristics. All the lasers in Table 4 have targeted the yellow–orange spectral region, with output wavelengths in the range 579–599 nm. Output pulse durations are in the range 3–45 ns, mostly at multi-kHz repetition rates. In terms of input–output characteristics, the lasers vary from a low-power (5.5 mW) orange laser pumped by a 1.6 W laser diode to a multi-watt (3.14 W) yellow laser side-pumped by a 99 W arrangement of diode bars. Also included in Table 4 are two examples of self-Raman lasers [60,61] and three examples where the same crystal is used for SRS and SHG [14,42,62].

Table 4
Summary of experimental parameters and performance of selected intracavity doubled intracavity Raman lasers

Pump source (configuration)	Laser crystal	Raman crystal (length)	SH crystal	SH output (wavelength)	Pulse duration (prf)	SHG efficiency	Ref.
3 kW arclamp (side pumped)	Nd:YALO	$LiIO_3$ (40 mm)	$LiIO_3$	685 mW (592 nm)	45 ns (4 kHz)	22% wrt Optimised fundamental	[14]
3 kW arclamp (side pumped)	Nd:YALO	$LiIO_3$ (40 mm)	$LiIO_3$	472 mW (592 nm)	11 ns (3 kHz)		[62]
3 kW arclamp (side pumped)	Nd:YAG	$LiIO_3$ (50 mm)	LBO	480 mW (578 nm)	30 ns (3 kHz)	28% wrt Optimised Stokes	[48]
2∼15 W 0.8 μm diodes, (double-end pumped)	Nd:YAG	$LiIO_3$ (50 mm)	LBO	1.2 W (578 nm)	30 ns (10 kHz)	22% wrt Optimised fundamental	[63]
1.6 W diode (end pumped)	Nd:YVO_4	$Ba(NO_3)_2$ (50 mm)	LBO	5.5 mW (599 nm)	6 ns (32 kHz)	0.34% wrt Diode	[64]
QCW diode 300 W/ 28.7 mJ (side pumped)	Nd:KGW	Nd:KGW	LBO	164 μJ (591 nm)	300 Hz	0.72% wrt Diode	[61]
QCW diode 120 W/ 14 mJ (side pumped)	Nd:KGW	Nd:KGW (25 mm)	LBO	93 μJ (591 nm)	<10 ns	0.8% wrt Diode	[60]
10 W diode (end pumped)	Nd:YAG	KTP (20 mm)	KTP	250 mW	18 ns (10 kHz)	2.5% wrt Diode	[42]
18 W diode (end pumped)	Nd:YAG	KGW (50 mm)	LBO	1.8 W	∼10ns (16 kHz)	8% wrt Diode	[57]
99 W diode bank (side pumped)	Nd:YAG	$BaWO_4$ (46.6 mm)	KTP	3.14 W	15 ns (10 kHz)	3.1% wrt Diode	[58]
10 W diode (end pumped)	Nd:YAG	GdVO4 (15 mm)	KTP	763 mW (587 nm)	3.8 ns (15 kHz)	7.6% wrt Diode	[65]

Our own initial developments of visible-based crystalline Raman lasers, following the early work by Ammann [14], commenced with the demonstration of an arclamp-pumped yellow Nd:YAG/$LiIO_3$/LBO laser. These experiments showed that thermal effects in the Raman crystal itself play a very important role in laser operation [48]. Using an interferometric method, we measured the strengths of the thermal lens in $LiIO_3$ and also $Ba(NO_3)_2$ and found the lens strength to scale with Stokes power density [66,67]. Making a transition to diode pumping with its much-increased brightness was found to result in even stronger thermal lenses [63], and we came to appreciate the challenges of engineering a system that included strong positive thermal lensing in the Nd laser crystal (focal length ∼12 cm) and strong negative thermal lensing in the $LiIO_3$ Raman media (focal length ∼−10 cm). We subsequently developed methods for resonator design that allowed the resonator to operate stably over a wide dynamic range from threshold up to the maximum designed input and output powers [15,68]. Given the highly dynamic nature of the optical

stability, it is not surprising that the resonator mode sizes in each crystal were found to vary considerably as the laser input power was increased to the operating point, and it can be quite challenging to design a simple resonator that enables both efficient optical conversion to the yellow and stable operating characteristics. Ultimately it was the thermal lens in the Raman crystal that limited the yellow output power from the system.

Fortunately in the past 15 years or so, a much wider range of Raman-active crystals has become available as practical alternatives to $LiIO_3$ and $Ba(NO_3)_2$, which, in addition to poor thermal characteristics, also had low threshold for optical damage. Particularly suitable and successful crystals include members of the monoclinic and tetrahedral tungstate groups (e.g. $KGd(WO_4)_2$ and $BaWO_4$) and the vanadates (e.g. $GdVO_4$ and YVO_4); their properties are tabulated in Table 1. Since many of these crystals can be doped with laser ions such as Nd^{3+}, they are also attractive for self-Raman laser configurations.

When our group investigated $KGd(WO_4)_2$ (KGW) as an alternative to $LiIO_3$, we found that thermal lensing was weaker by an order of magnitude, which is consistent with its higher thermal conductivity and lower thermo-optic coefficient. In a direct comparison [69] of yellow lasers based on $LiIO_3$ and KGW, KGW having much better thermal properties (see Table 1) and therefore much weaker thermal lensing, we found that the $LiIO_3$ laser produced a maximum output of 1.4 W at 578 nm, limited by thermal lensing in the Raman crystal, while the KGW laser produced a maximum of 1.7 W at 579 nm, limited by thermal lensing in the laser crystal. KGW was also found to be particularly robust in terms of optical damage.

The highest yellow–orange output power obtained from a crystalline Raman laser has been reported by Li et al. [58] in 2007. A maximum output of 3.14 W was obtained at 590 nm from a diode side-pumped (99 W) Nd:YAG module, AO Q-switched at 10 kHz. The Raman crystal was a 46.6-mm-long piece of $BaWO_4$ and the doubling crystal was KTP. The side-pumped configuration used, although not usually as efficient as end-pumping, does simplify power scaling. At the maximum pump power level of 99 W, the authors measured strong thermal lensing, and the use of a plane-convex resonator to reduce the effect of strong lens was found to provide better overlapping of the fundamental and Raman beams in the Raman crystal. The KTP doubling crystal, while having a high d_{eff}, also has a high (2°) walk-off, which reduces the overlap of the o- and e-polarized beams. The plano-convex resonator provides a larger spot in KTP, thereby increasing overlap efficiency. The best overall diode-to-yellow efficiency was 3.2%. However, as Li et al. note, higher powers and efficiencies should be possible with a folded resonator design that enables the yellow light generated in both directions to be captured.

In 2005, Chen reported a compact (90 mm overall length) yellow laser, end-pumped by a 10 W diode laser that employed Nd:YAG as the laser crystal and a single 20 mm-long KTP crystal as both the Raman and doubling media [42]. The maximum yellow output was 0.25 W at 548 nm, with 1.03 W at the second-Stokes wavelength of 1129 nm also being present.

Very recently, Li et al. reported a small-scale and very efficient yellow laser based on a 4-mm-long Nd:YAG laser crystal, 30 mm-long AO Q-switch, 15 mm-long Nd:$GdVO_4$ Raman crystal and 6 mm-long KTP crystal [65]. Placed in close proximity between a 1 m concave input mirror and a plane output mirror, and end-pumped by a 10 W diode laser at 808 nm, this laser produced 763 mW at 587 nm. The output pulses were around 3.8 ns duration at 15 kHz. It was noted that their optimisation process involved varying the KTP orientation to compensate the effects of changes to the fundamental and Stokes

polarisation that occurred when these beams passed through the KTP. The authors also note that their output mirror was lossy ($T\sim7\%$) for the first Stokes, and that only the yellow generated in one direction was collected. Consequently, higher powers and efficiencies should be possible with an optimised resonator.

4.2. Wavelength-selectable pulsed lasers

4.2.1. Design principles

The design principles associated with fixed-wavelength lasers in Section 4.1 also apply to the wavelength-selectable lasers considered here. In addition, careful consideration needs to be given first to controlling the cascading of the Stokes orders and second to selecting a nonlinear crystal to tune over the relatively broad wavelength range.

As presented in Section 2, it is the cascaded nature of the SRS process that can be utilised to generate wavelength-selectable output at visible wavelengths in the green–yellow–red spectral region. Given sufficiently broad mirror coatings, the fundamental, first, second and potentially higher-order Stokes wavelengths can all be resonated. For wavelength-selectable output to span the green–red spectral region, mirrors with high reflectivity from around 1060 to 1300 nm are required. The fabrication of such mirrors, with added constraints of high threshold for optical damage, high transmission at diode-pump wavelength (mirror M1) and high transmission (M2) or reflectivity (M3) at visible wavelengths, is feasible but requires customised coating runs, which are expensive.

4.2.2. Review of selected results

To our knowledge, wavelength-selectable lasers based on intracavity SHG/SFG of intracavity Raman lasers have been reported only by Ammann [14,62] and ourselves [57,69].

In the experiments of Ammann, the highest outputs were achieved at 540 and 592 nm, the second harmonics of the fundamental and first-Stokes wavelengths, respectively. Output at 657 nm was much lower, most probably because the resonator mirrors were partly transmitting at the second-Stokes wavelength of 1.31 μm. Output produced by sum-frequency mixing of the fundamental and first-Stokes frequencies was quite low compared to the second harmonics, probably resulting from competition between the SRS and SFG processes. Output produced by sum-frequency mixing of first and second Stokes was similarly low. It is interesting to note that the frequency spacing between the Stokes orders was not uniform. This is because $LiIO_3$ is a polar uniaxial crystal, and for the crystal orientation used, the Raman shift is determined by an oblique phonon mode, a characteristic of which is that the frequency shift is a function of the angle between the optical axis and direction of propagation [70]. Consequently, as the crystal was rotated to tune the phase-matching conditions, the frequency shift also changed.

In our own work, we see a similar spread of output powers across the wavelengths observed. Lower output powers were obtained at longer wavelengths, because both the resonator mirrors were 20–30% transmitting at the second-Stokes wavelength (1273 nm). We also found that the powers generated at the sum frequencies were lower than that at the second harmonics [57].

There are several means that can be employed for wavelength selection, and in each case there are tradeoffs involved in the system design. By way of example, angle tuning the nonlinear crystal can give rapid switching (e.g. on ms timescales) between selectable

wavelength, but active control of an output mirror is most likely required to maintain cavity alignment. On the other hand, temperature tuning offers full electronic control over the output wavelength; however, the time to tune between different wavelengths is likely to be slow (~1 min). BBO is the most promising candidate for angle tuning, while LBO is the most promising candidate for temperature tuning. KTP is the most efficient and low-cost frequency-doubling crystal, but its phase-matching properties are not consistent with angle or temperature tuning for this application.

We have investigated three different means for achieving wavelength selectability: angle and temperature tuning in LBO, and angle tuning in BBO. The results for each method are summarised in Table 5. In each case, the pump power was in the range 18–23 W and the repetition rate was 12 kHz.

Angle tuning of BBO: BBO is suited well for wavelength selection by angle tuning because only small angles are required to tune between consecutive wavelengths. A 4 mm-long BBO crystal cut for critical phase matching ($\theta = 21.7^\circ$) of the 1158/579 nm interaction was used in Ref. [69] to generate wavelength-selectable output at the four wavelengths as shown in Table 5. These wavelengths were obtained by accessing the 768 cm^{-1} Raman shift in the KGW crystal; a second set of four wavelengths could be accessed using the 901 cm^{-1} Raman shift. The angle through which the crystal was rotated was approximately 3°, and only minimal realignment of the cavity was required.

Angle tuning of LBO: In comparison to BBO, substantially larger tuning angles are required to select between different visible wavelengths. A 10 mm-long LBO crystal was used in Ref. [57], cut for critical phase matching of the 1158/579 nm interaction. Output at 579 nm was obtained near normal incidence, and outputs at 555 and 579 nm were achieved by rotating the crystal through an angle of approximately 11° and 17°, respectively, followed by realignment of the output mirror. The output powers and calculated angles for phase matching [41] are summarised in Table 5.

Temperature tuning: For temperature tuning across four visible wavelengths [57], two 10 mm-long LBO crystals were used, each with an independent temperature controller. Crystal LBO1 was cut for non-critical phase matching ($\theta = 90^\circ$, $\varphi = 0^\circ$), while crystal LBO2 was cut for critical phase matching of the 1064/532 nm interaction at 25 °C. Green output was obtained when LBO2 was tuned to 25 °C. To obtain output at other wavelengths, LBO2 was held at 52 °C, and LBO1 was tuned between 19 and 95 °C to

Table 5
Summary of output powers and configurations of the SFG/SHG crystal(s) used to obtain wavelength-selectable output

Selection method	532 nm	555 nm	579 nm	606 nm
Angle-tuned BBO [69]	1.3 W $\theta_{calc} = 22.8^\circ$	0.5 W $\theta_{calc} = 22.2^\circ$	1.1 W $\theta_{calc} = 21.7^\circ$	0.28 W $\theta_{calc} = 21.1^\circ$
Angle-tuned LBO [57]	1.7 W $\varphi_{calc} = 11.4^\circ$	0.95 W $\varphi_{calc} = 8.5^\circ$	1.8 W $\varphi_{calc} = 5.3^\circ$	–
Temperature-tuned LBO [57]	1.5 W T1 = 95 °C T2 = 25 °C	0.52 W T1 = 95 °C T2 = 52 °C	0.57 W T1 = 48 °C T2 = 52 °C	0.20 W T1 = 19 °C T2 = 52 °C

Note: θ_{calc} and φ_{calc} are phase-matching angles calculated using SNLO [41].

obtain output at 555, 579 and 606 nm. In principle, phase matching can also be achieved in LBO1 for 532 nm (by increasing its temperature to 150 °C), but this would require a multi-stage TEC.

The lower optical efficiencies obtained for temperature tuning are attributed to the increased insertion loss of the second LBO crystal and the effect of additional resonator length on the pump-resonator mode overlap in the Nd:YAG rod. Recently TECs that operate up to 200 °C have become available and temperature tuning across a wider range of wavelengths (including 532 nm) may be possible with a single LBO crystal with temperature controlled by a multi-stage TEC.

5. CW intracavity Raman lasers with intracavity SHG

While CW fibre-based Raman lasers have been well known for many years [71], the development of other forms of CW Raman lasers is quite recent. CW Raman lasers based on H_2 gas using very high finesse optical cavities were first developed in 1998 [72], and all-silicon CW Raman lasers were first reported in 2005 [73]. Efficient CW operation in diode-pumped intracavity Raman lasers was considered unlikely (due to the high intracavity fields required in order to initiate the SRS process) until in 2004 when Grabtchikov et al. [74] demonstrated a CW Raman laser employing barium nitrate in an external resonator pumped by an argon ion laser at 514 nm. In the following year, Demidovich et al. [75] and Pask [76] reported CW diode-pumped intracavity Raman lasers, while the first CW self-Raman laser based on Nd:YVO_4 was published by Burakevich et al. [77] in 2007.

In previous sections, we have seen efficient visible light generation is possible in intracavity frequency-doubled Q-switched Raman lasers, with diode-to-yellow conversion efficiencies approaching 10%. In this section, we detail the design principles and present work on CW yellow Raman lasers with comparable conversion efficiencies.

5.1. Design principles

The key design challenge for CW Raman lasers is to reach threshold even when an intracavity configuration is used. Obtaining low Raman thresholds requires the use of high-Q cavities and maintaining small-diameter modes in the Raman medium; hence high-intensity cavity fields are usual. This in turn dictates the use of high-damage-threshold coatings. Despite the tight constraints, relatively low CW Raman thresholds have been attained in diode-pumped systems mostly due to the availability of high-brightness laser diodes as well as ultrahigh-reflectivity high-damage-threshold laser mirrors.

The diode-pump power P_P required to reach Raman laser threshold can be written as [78]

$$P_P = \frac{A_R}{\eta g_R l_R} \frac{(T_S + L_S)(T_F + L_F)}{4} \tag{4}$$

where A_R is the area of the intracavity beam in the Raman crystal, g_R and l_R are the Raman gain coefficient and length of the Raman crystal, respectively, η is the ratio of diode-pump and fundamental laser photon energies, and $(T_F + L_F)$ and $(T_S + L_S)$ are the sum of the output coupling and round trip losses for the fundamental and Stokes wavelengths, respectively. This equation assumes that the inversion in the laser crystal is

efficiently extracted. This is normally the case for such high-Q cavities in which the laser intensity is much higher than the saturation intensity for the laser material.

Actually, relatively modest diode-pump powers are required once the cavity loss and mirror transmissions have been suitably reduced. Consider an Nd:YVO_4 laser (pumped by an 808 nm laser diode) with an intracavity KGW crystal. For realistic values of total round trip losses of order 1%, $l_R = 2.5\,\text{cm}$, $g_R = 5 \times 10^{-11}\,\text{m/W}$ and $A_R = \pi(150 \times 10^{-6})^2\,\text{m}^2$, we calculate a threshold pump power of 1.9 W. Reducing the resonant mode size, for example, to 95 μm diameter, the threshold decreases to just 190 mW, making low-power yellow laser sources certainly practical.

For CW infrared Raman lasers designed to output at the first-Stokes wavelength, a small output coupling of the order of 1% was found to be appropriate [78]. Such a small value means that nonlinear output coupling of the Stokes optical field through intracavity frequency doubling is well suited for extracting the Stokes power efficiently. Cavities with minimised losses and mirror transmission at the fundamental and Stokes wavelengths can be employed to achieve low Raman thresholds. The doubling process does not extract any power at the threshold, resulting in the lowest possible Raman threshold. As the Stokes field increases in power, the fraction doubled per round trip increases, and a strong doubled-Stokes beam may be generated with high efficiency.

5.2. Review of selected results

Table 6 summarises the experimental parameters and results of four different intracavity-doubled CW Raman lasers. The basic scheme for all of these is shown in Fig. 5.

In the first report of an intracavity-doubled CW Raman laser [79], Nd:$GdVO_4$ was used as the laser crystal, a 25 mm length of KGW as the Raman media and LBO for second-harmonic frequency conversion. The crystals were positioned close together, and the resonator formed by a flat input mirror and a 200 mm concave output mirror.

Table 6
Summary of performance and experimental parameters for selected CW intracavity-doubled intracavity Raman lasers

Diode pump power (W)	Laser crystal (length)	Raman crystal (length)	Doubling crystal (length)	Threshold (W)	Max. output at 100% d.c. (50% d.c.)	Max. efficiency at 100% d.c. (50% d.c.)	Ref.
30	Nd:$GdVO_4$ (10 mm)	KGW (25 mm)	LBO (10 mm)	2.5	704 mW(1.57 W)	5.1 (7.9)	[79]
30	Nd:$GdVO_4$ (10 mm)[a]	Nd:$GdVO_4$ (10 mm)[a]	LBO (10 mm)	2.4	678 mW(1.88 W)	4.2 (7.2)	[80]
4.5	Nd:YVO_4 (10 mm)[a]	Nd:YVO_4 (10 mm)[a]	LBO (10 mm)	2.1[c]	140 mW[c]	4.4[c]	[81]
4.5	Nd:YVO_4 (3 mm)[b]	Nd:YVO_4 (10 mm)[b]	LBO (10 mm)	0.8	115 mW	2.6	[82]

Performance in some experiments is for true CW i.e. 100% duty cycle (d.c.) and for 50% d.c.

[a]Self-Raman configuration.

[b]A segmented self-Raman crystal with 3-mm-doped length.

[c]Near-concentric resonator configuration. All other configurations were short cavities.

The output of this laser depended critically on the output coupling and in particular on other "non-useful" resonator losses. With mirrors having 0.8% coupling loss at the Stokes wavelength, the yellow power was limited to 320 mW. Mirrors with higher reflectivity (a total transmission at 1176 nm of only 0.008%) resulted in the yellow power increasing to over 704 mW for a diode power incident on the laser crystal of 13.7 W. The threshold pump power for this system was correspondingly reduced from 6.9 W to around 2.5 W. The output powers reported were limited by thermal lensing, primarily in the laser crystal. Above 14 W pump power, the output power decreased as strong thermal lensing in the laser crystal caused the resonator to become unstable. However, by operating the pump diode at 50% duty cycle (d.c.), and thereby reducing the thermal lens by a similar proportion, instantaneous output powers (during the on cycle) reached 1.57 W for an instantaneous diode power (during the on cycle) of 19.9 W. Laser characteristics of this "three-crystal" (Nd:$GdVO_4$/KGW/LBO) laser operating at 100% d.c. and at 50% d.c. are shown in Fig. 6. We also note that the yellow light was collected only from the output coupler and no account of the backward propagating light was made.

It was apparent that further improvements to the performance of the CW yellow laser could be achieved if the thermal lensing could be managed better and if resonator losses could be reduced further [79]. A numerical modeling study [78] was carried out to investigate which parameters had the greatest impact on the efficiency of the laser system. This work suggested potential for improvement by redesigning the laser system, for example, by increasing the strength of both Raman shifting and nonlinear conversion. These increases might be achieved by designing a resonator with smaller spot sizes in the

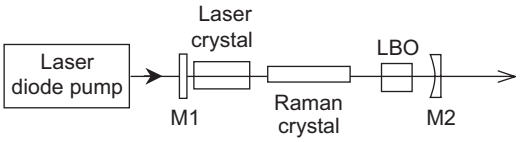

Fig. 5. Experimental arrangement for an intracavity-doubled CW Raman laser.

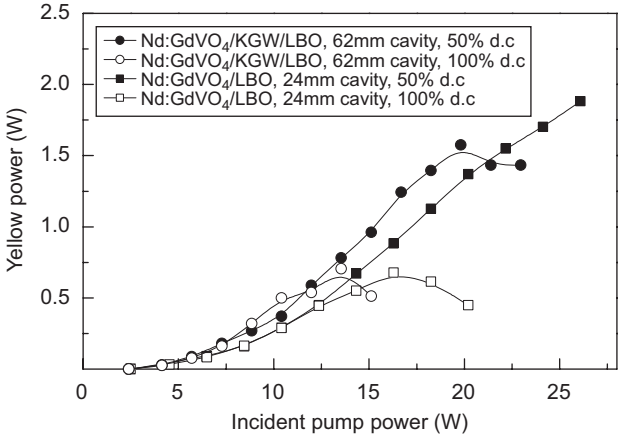

Fig. 6. Yellow output powers as a function of diode pump power for the three-crystal Nd:$GdVO_4$/KGW/LBO Raman laser and Nd:$GdVO_4$/LBO self-Raman laser [79,80].

Raman and doubling crystals, increasing the length of these crystals or using materials with larger nonlinear coefficients. Increasing the pump power will also lead to increases in efficiency and hence large increases in output power. Decreasing the remaining cavity losses can have a substantial impact—for the laser using 0.008% output coupling at 1176 nm, it is estimated that the effective output coupling of the doubling crystal was just 0.7%, and so clearly the round trip losses of over 1% severely decrease the laser efficiency. The model suggests that halving the losses to 0.5% would result in nearly a doubling of the laser efficiency.

Dekker et al. [80] also used the same 10 mm-long Nd:$GdVO_4$ crystal in a self-Raman configuration (i.e. the KGW was removed from the cavity), since one less crystal would clearly reduce non-useful cavity losses, and also enabled a shorter cavity, which is beneficial for accommodating the strong thermal lens. The threshold was slightly less than in the three-crystal system described earlier (2.4 vs. 2.5 W) despite the fact that the self-Raman medium was only 10 mm long compared to the 25 mm-long KGW crystal. For comparison, the laser characteristics of the self-Raman (Nd:$GdVO_4$/LBO) laser operating at 100% d.c. and at 50% d.c. are also plotted beside the three-crystal results in Fig. 6. As the Raman gains of these two materials are reported to be similar [23], this clearly demonstrates the importance of reducing the overall losses as a means of reducing the Raman threshold. In this arrangement the maximum visible output power (at 586 nm) was 678 mW, achieved for a diode power of 16.3 W. For higher pump powers, the yellow output power again maximised and then decreased, as the thermal lens strength in the Nd:$GdVO_4$ crystal pushed the resonator into the unstable regime. Once again, when the diode pump was modulated at a 50% d.c. in order to reduce the thermal load, the maximum yellow output power increased markedly, up to 1.88 W (instantaneous output power) with no rollover up to the maximum available pump of 26 W. Since the linear cavity permitted collection of the yellow light generated only in one direction, we anticipate that the yellow power actually generated was twice this, at around 3.76 W, with a diode-to-yellow conversion of 14.5%. Such high conversion efficiencies, which exceed the best reported for Q-switched operation [83] by almost 5%, are due to the low level of residual losses of the CW self-Raman system.

It is interesting to note that the thermal lens, and hence maximum achievable output power in a plano/plano resonator, in the intracavity-doubled self-Raman system is stronger than in the three-crystal system described earlier. In the intracavity-doubled self-Raman laser, thermal loading arises from diode pumping, the inelastic nature of the Raman process and the reabsorption of the backward-propagating yellow emission. The Raman conversion process, in the reports detailed above, is calculated to contribute to approximately 25% of the overall thermal lens. It should also be noted that the thermal loading in Raman systems with high-Q cavities is substantially higher than expected and has been attributed to effects such as impurity absorption. The result of the increased thermal lens strength is normally associated with a decrease in the maximum possible pump power, although in the self-Raman system this is offset by the reduced cavity length accommodating stronger thermal lenses.

Despite these promising early results there remain some serious challenges in obtaining high-power (3–5 W), high-beam-quality and efficient (~10% diode-to-yellow) CW operation. For example, the beam quality of the yellow emission was reported [80] to be relatively poor with M^2-values of 5–6 at maximum pump powers. As discussed, the major problem lies with thermal loading in the Nd:$GdVO_4$ crystal, making transverse mode

control difficult. Possible strategies to reduce the thermal loading and hence the induced lens include redirecting the yellow light using an L-shaped cavity or compensating for the lens using a convex–concave resonator. Alternatively it may be simpler to power scale using a three-crystal cavity separating the fundamental and Raman processes, for example in a z-fold resonator.

There is considerable interest in low-power yellow lasers, e.g. for biomedical lasers. Given that thresholds around 2.4 W had already been achieved, we decided to test the feasibility of low-power yellow lasers pumped by a high-brightness 4.5 W laser diode, which was focused to a spot around 160 μm (average of two absorption lengths) in the laser crystal. A self-Raman configuration was employed in Ref. [81] with a 10 mm-long Nd:YVO_4 crystal and a 10 mm-long LBO crystal used as a nonlinear output coupler. Using a short linear cavity, in which all the crystals were closely packed in a resonator formed by a flat input mirror and an output mirror with a 10 cm radius of curvature, up to 92 mW was obtained for 4.2 W diode power incident on the laser crystal. The beam was measured to have an M^2-value of ~3.

In an effort to improve the beam quality, a near-concentric resonator was then used [81], in which small changes to the cavity length caused large changes in resonator mode size, so that the resonator mode in the laser crystal could be optimally mode matched to the pumped volume. In this case, a maximum yellow output of 140 mW was achieved with high beam quality (M^2-value of 1.2). This approach does however require the pump power to remain relatively fixed as the cavity is only optimised for one power level.

Most recently, Omatsu et al. [82] investigated a composite Nd:YVO_4/YVO_4 self-Raman laser in order to reduce the thermal lens strength. The composite crystal cavity with an intracavity LBO crystal as a nonlinear output coupler delivered a maximum of 115 mW output at 589 nm. Most of the diode power was absorbed in the back (Nd-doped section) 3 mm of the crystal; however, the entire 10 mm length of the crystal was available for SRS. The input face of the crystal was also directly coated with a high-reflectivity coating. The anticipated advantages of this arrangement were that thermal lensing should be reduced by the end cap. Indeed thermal lensing was slightly (~10%) weaker. Up to 115 mW was obtained in the short linear cavity, compared to 90 mW obtained earlier in Ref. [81], and no rollover in output power was observed up to the maximum available pump power of 4.2 W.

All of the results regarding CW visible laser operation discussed so far are obtained from SHG of the first-Stokes emission. In principle, visible output in the green or further into the red is possible by cascading the Stokes emission and using a temperature- or angle-tuned SFG crystal to couple out the desired visible output, similar to that already demonstrated in Q-switched Raman laser systems [57]. To date, CW second-Stokes output has been obtained only with low-power ~20 mW and high-threshold pump powers (3.6 W) [84], making frequency doubling impractical. With improved coatings however, significant visible output powers of the second Stokes and beyond appear within reach.

We believe that by managing the thermal loading and collecting all the generated yellow emission, CW intracavity-doubled Raman laser output powers in the 3–5 W range can be achieved at >10% diode-yellow conversion efficiencies. Overall, the simplicity of the laser configuration (either three optical components or two in the self-Raman system) gives the potential to make very compact devices based on readily available components, and the flexibility to produce different output wavelengths through the choice of different laser and Raman materials.

6. External-resonator Raman lasers

In this section, visible wavelength generation using external-cavity Raman lasers is reviewed. Studies to date have largely used frequency-doubled Q-switched Nd-doped lasers as pump sources; copper vapour [46] and CW Ar^+ ion pump lasers [74] have also been used. With the variety of pump sources and Raman materials, several tens of wavelengths in the range 540–800 nm have been reported. The advantages of the external-resonator architecture are discussed along with details of key achievements in targeting single- and multi-wavelength outputs.

6.1. Basic design characteristics

The external-cavity Raman laser in its most basic embodiment consists of an input coupler that is highly transmitting at the pump wavelength and highly reflecting at the Stokes wavelengths, and an output coupler partially transmitting at the output Stokes wavelength, as in Fig. 1b. The output coupler is often reflective at the pump wavelength to provide up to a two-fold enhancement of the pump intensity in the Raman crystal. The curvature of the resonator optics and the parameters of the pump beam should be selected to maximise pump and resonator mode overlap. Note, however, in some cases the gain can be very high and unstable resonators can be used to improve beam quality [44,85]. The gain volume in the resonator is most often dictated by the power and beam characteristics of the pump laser and typically the Raman-active material is chosen such that its length is equal to the confocal length of the pump beam. In Raman crystals such as $Ba(NO_3)_2$, $LiIO_3$ and metal tungstates, dimensions of 1 cm aperture and several centimeters to 10 cm long are available. In high peak power density lasers such as flashlamp-pumped Q-switched systems, beam waist sizes up to several millimeters are used while multi-kilohertz diode-pumped pump lasers are often focused down to as small as 100 μm diameter to achieve sufficient Raman gain.

A major attraction of the visible-pumped external resonator is that it can be a simple add-on to an unmodified visible pump source, thus allowing the approach to leverage available visible laser systems as pump sources. Pumping in the visible is convenient for several reasons. Higher single-pass gains are possible compared to infrared pumped counterparts due to a higher Raman gain coefficient. According to theory, the Raman gain coefficient scales by $1/\lambda_s$ [19]; however, there is a discrepancy between this relationship and experimental determinations of the Raman gain coefficient as noted in Ref. [15] and apparent in Table 1. An additional factor of $1/\lambda_p$ can be obtained owing to the longer Rayleigh range for the same focal spot size at shorter wavelengths, permitting the use of longer crystals. Moreover, higher maximum first-Stokes conversion efficiencies are possible due to the smaller quantum defect.

The external-resonator concept also lends itself to a system that can be configured for single-wavelength operation or to provide multiple Stokes lines simultaneously. The spectral content of the output depends on the resonator losses for each of the Stokes Raman orders. The output coupler reflectivity is most often used to constrain output to a selected Stokes order or provide multiple-wavelength operation. In fact, unless the output coupler spectral characteristics are carefully selected, more than one Stokes order is generally present in the output.

6.2. Review of selected results

The performance characteristics of many external-resonator Raman lasers are summarised in Table 7 along with details of the pump source, the conversion efficiency, and the output pulse energy and/or average power. To date, the highest conversion efficiencies from the pump beam to a selected Stokes order is about 50% and have been obtained using Q-switched pump lasers of pulse duration approximately 10 ns and using

Table 7
Summary of performance of selected visible pumped external cavity Raman lasers

λ_p (nm)	Pump pulse duration full-width-half-maximum (ns)	Pulse repetition frequency (Hz)	Raman crystal material	Principal Stokes output wavelength (nm) {Order}	Max. Stokes conversion efficiency (%)	Max. pulse energy (mJ)	Max. output power (W)	Ref.
532	10	–	$Ba(NO_3)_2$ $NaNO_3$ $CaCO_3$	– {1–4}	65[a]	–	–	[83]
532	6	1–30	$Ba(NO_3)_2$	563 {1}	40	25	0.75	[86]
				599 {2}	48	32	0.9	
532	(~0.5)	1.0×10^8	$CaWO_4$	589 {2}	–	1.0×10^{-4}	8–10[c]	[87]
578	20	<100?	$Ba(NO_3)_2$	615 {1}	~10	–	–	[88]
532	6	10	$PbWO_4$	559 {1}	13	1	0.01	[89]
527	400	1.0×10^3	$BaWO_4$	544 {1}	1.7	0.13	0.130	[90]
				583 {2}	0.8	0.022	0.022	
523.5	50	10^3	KGW	600 {3}	3.2	0.008	0.080	[91]
532	10	5×10^3	KGW 768 cm^{-1}	555 {1}	15	31.4×10^{-3}	0.157	[92]
				578 {2}	25	49×10^{-3}	0.245	[92]
				578 {2}	41	168×10^{-3}	0.84	[83]
				606 {3}	11	20.2×10^{-3}	0.101	[92]
				636 {4}	6	12.4×10^{-3}	0.062	[92]
532	10	5×10^3	KGW 901 cm^{-1}	559 {1}	22	46.4×10^{-3}	0.232	[92]
				589 {2}	35	71.2×10^{-3}	0.356	[92]
				589 {2}	45	210×10^{-3}	1.05	[83]
				622 {3}	20	38.8×10^{-3}	0.194	[92]
				658 {4}	14	30.8×10^{-3}	0.154	[92]
532	20	10	$Ba(NO_3)_2$	563 {1}	19	34	0.34	[44]
				563 {1}	20.3	0.69	0.69	[93]
				599 {2}	35.3	1.19	1.19	[93]
				634 {3}	18.7	0.6	0.60	[93]
532	105	1.0×10^3	$Ba(NO_3)_2$	685 {4}	7	0.2	0.22	[93]
				737 {5}	11.5	0.4	0.40	[93]
				799 {6}	5.7	0.19	0.19	[93]
532[b]	190	1.0×10^3	$Ba(NO_3)_2$	599 {2}	40	0.6	0.60	[93]
514	CW	CW	$Ba(NO_3)_2$	543 {1}	5	NA	0.164	[74]

Note that where several Stokes orders are listed, the output performance corresponds to laser resonator configurations more optimal for that Stokes order.

[a]Sum of conversion efficiencies to first four Stokes orders.

[b]Line-narrowed pump source.

[c]Limited results presented.

materials $Ba(NO_3)_2$ and KGW. He and Chyba [86] reported a conversion efficiency of 48% to 599 nm (second Stokes) using a flashlamp-pumped frequency-doubled Nd:YAG laser pulse of duration 6 ns in $Ba(NO_3)_2$ at average powers up to 900 mW. Using a different output coupler, 40% conversion to the first Stokes at 563 nm was obtained at 750 mW output power. Mildren et al. [83] reported 45% conversion to the second Stokes (589 nm) for a KGW Raman laser pumped with 10 ns pulses at 532 nm at a pulse rate of 5 kHz and an average output power of 1.05 W. From an overall survey of the above results, it is interesting to note that the conversion efficiencies are often highest for the second Stokes, despite the higher quantum defect. This is explained by coating constraints as the spectral requirements for the output coupler, which are optimally reflective at the pump wavelength and partially reflective at the output Stokes, are easier to satisfy for second Stokes.

When considering the total conversion to multiple-Stokes lines, the efficiencies are notably higher. The earliest external-cavity Raman laser demonstrations by Karpukhin and Stepanov [85], which employed $Ba(NO_3)_2$, $NaNO_3$ and $CaCO_3$ and a Q-switched 532 nm pump laser, reported overall conversion efficiencies to the Stokes of up to 65%. Mildren et al. [83] demonstrated 64% conversion to combined second and third Stokes (589 and 621 nm) for the 901 cm^{-1} Raman shift of KGW. As shown in Fig. 7a, the output power for this system increased linearly with input power at a slope efficiency of approximately 78% up to the maximum output power of 1.5 W. At the maximum output power, the output consisted of approximately 70% at 589 nm and the remainder at 621 nm (Fig. 7b). The output spectrum changes notably depending on the orientation of the crystal with respect to the pump laser due to the presence of the 768 cm^{-1} Raman mode. When the pump was orthogonally polarised, the output spectrum consisted of lines involving the 768 and 901 cm^{-1} Raman modes (578, 589, 606, 611 and 621) at a slightly lower overall conversion efficiency (58% maximum).

Several studies have investigated conversion for pump pulses of duration substantially longer than 10 ns. In one such report Vodchits et al. [93] achieved 35% conversion efficiency from 532 nm to 599 nm in $Ba(NO_3)_2$) using 105 ns pulses at the pulse rate of 1 kHz. It was also shown that line narrowing the pump laser can markedly reduce the Raman laser threshold and increase conversion efficiency. For example, by reducing the

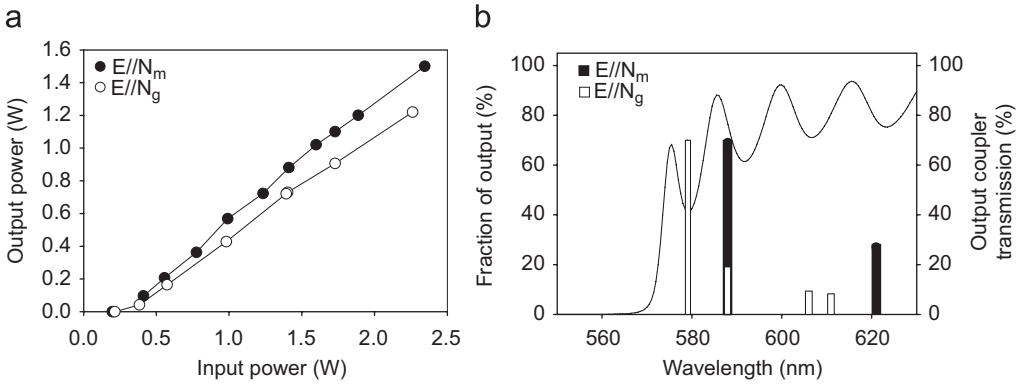

Fig. 7. (a) Laser output characteristic and (b) corresponding spectral content for a KGW external resonator Raman laser pumped at 532 nm at 5 kHz. The output coupler transmission curve is also shown, along with output for pump polarisation aligned with the two crystal-optic axes Nm and Ng.

pump linewidth to 0.14 cm^{-1} (using a 3 mm etalon placed inside the pump laser oscillator), a reduction in the threshold power from more than 1.9 to 0.41 kW and a two-fold increase in the conversion efficiency to 40% were observed. Interestingly, conversion efficiencies reported for frequency-doubled Nd:YLF pump lasers are all relatively low to date. For 527 nm pump pulses of duration ~400 ns in $BaWO_4$, Zverev et al. [90] reported 1.7% conversion to first Stokes and 0.8% to the second Stokes. Our own studies, using a 523.5 nm Nd:YLF pump laser of pulse duration 50 ns and 10 kHz, generated 81 mW of predominantly third Stokes at 600 nm at a conversion efficiency of 3.2% [91]. Recently, a crystalline external-cavity Raman laser was demonstrated in the CW mode for the first time by Grabtchikov and co-workers [74,94]. Using a 514 nm Ar^+ pump laser and a high-Q Stokes resonator, they achieved approximately 5% conversion to the 543 nm first Stokes in $Ba(NO_3)_2$. They also observed weak emission at 488 nm [94], which they attributed to anti-Stokes generation.

Most work to date has concentrated on achieving efficient conversion to a selected Stokes order; however, there are applications that demand powerful output on several well-spaced wavelengths in the visible. By replacing the output coupler in the resonator [83], we have demonstrated a KGW Raman laser generating up to four Stokes wavelengths in the range 555–660 nm simultaneously with each component capable of over 130 mW output power, and with a total output power of 1.7 W (see Fig. 8). The power input from the 5 kHz 532 nm pump was 2.36 W and the output coupler transmission had approximately 50% transmission for the pump laser and for each Stokes order. The concentration of output on each Stokes order can be tailored to the specific application using an output coupler spectral profile with reduced transmission at the pump and lower-order Stokes.

External-cavity Raman lasers have been studied for a number of applications, including medical and guide stars as well as environmental sensing. Development of 589 nm sodium-layer laser guide stars based on Raman shifting has addressed interesting challenges in

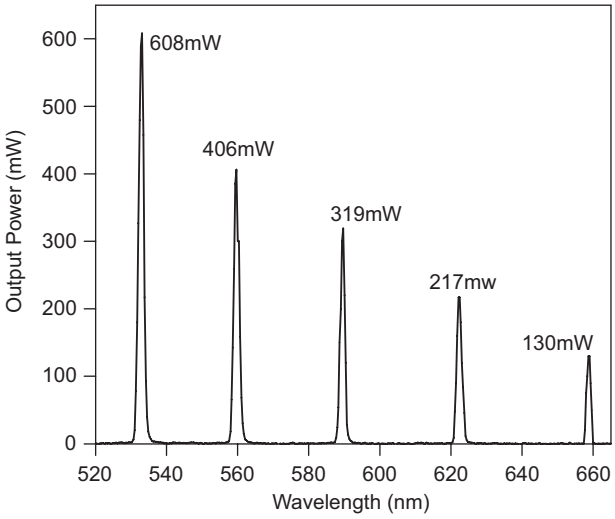

Fig. 8. Output spectrum of a 532-nm-pumped KGW Raman laser with an output coupler selected to provide multi-wavelength operation [83]. The input power transmitted by the input coupler was 2.36 W.

order to satisfy the tight constraints on output power, wavelength, bandwidth and the spatio-temporal properties needed for this application. For example, using two Raman crystals positioned in the waists of a bowtie resonator, pulses ~0.5 ns in duration at pulse rates of 100 MHz and with bandwidth 0.75–1.0 GHz were generated using $CaWO_4$ in an external-cavity Raman laser with the wavelength closely matching the 589.0 nm sodium D_2 line [87,95,96]. The target output power was 10 W, though the maximum output power achieved was never reported to our knowledge. A major challenge of this work was to shift the Nd:YAG laser output wavelength by approximately 0.4 nm needed to obtain precise overlap with the atomic transition. The group investigated temperature tuning of the Nd:YAG medium as well as using co-dopants. A guide star scheme also involving Nd:YAG and $CaWO_4$ was patented around the same time by TRW, Inc. [97]. The General Physics Institute (Moscow) showed that a similar spectroscopic coincidence with the D_2 line is achieved using a $BaWO_4$ Raman laser pumped by the second harmonic of a Nd:GGG laser, where the latter was heated above ambient temperature to improve spectral overlap [98,99].

Remote-sensing applications which target the atomic lines of atmospheric constituents have led some researchers to study line narrowing of the Raman laser output using etalons placed inside the Raman laser resonator [88,97], though again very little details of this work have been published. Work at Clarendon Labs at the University of Oxford aimed at generating output near 616 nm using a $Ba(NO_3)_2$ external-cavity Raman laser pumped by a 578 nm copper vapour laser for applications in atmospheric sensing of OH at the second harmonic [88]. They found that etalons introduced large losses and concluded that the output spectral width was dominated by the pump spectrum.

Other work includes schemes to diversify the choice of output wavelengths from Raman lasers. The selection of target wavelengths is also significantly boosted for materials that have more than one active Raman mode [92,100]. Recently, it has been shown that the number of output wavelength choices increases many-fold for Raman materials like KGW, which can be oriented to provide high gain on two Raman modes simultaneously [100]. The output wavelengths include the Stokes order corresponding to each Raman mode as well as Stokes orders involving combinations of each mode. Up to 11 visible Stokes lines were observed in the 550–700 nm range, in contrast to only four lines for a single-Raman mode. This has implications for also expanding the possible wavelength options when generating UV output via SFG as discussed in the following section.

Since the first report in 1986, an extensive body of knowledge on materials and pump sources has been built and commercial visible external-cavity Raman lasers have been available for many years (e.g. Solar Laser Systems, Minsk, Belarus). Relatively straightforward model simulations have been able to reproduce basic performance characteristics in pulsed [101] and CW [94] regimes. However, there is substantial scope for further scaling performance of these systems, and importantly the average output power. To date, the reported output powers have been chiefly limited by the power of the pump sources used and there is little evidence that thermal effects impact on performance (though thermally induced birefringence was noted to be significant in a $Ba(NO_3)_2$ Raman laser of output power approximately 1 W [56]). Visible $Ba(NO_3)_2$ Raman lasers and KGW Raman lasers have been scaled up to 0.9 W [86] and 1.5 W [83] of Stokes output power, respectively, without rollover. Despite this, non-standard architectures have been proposed that mitigate against thermal effects such as non-collinearly pumped Raman lasers [102], multiple crystal configurations [87] and zig-zag slab designs [103]. Efficiency may also be

boosted by consideration of the pump laser spectral width as highlighted in the aforementioned recent study by Vodchits et al. [93]. The scope for increasing output power capability is thus substantial. Given the straightforward adaptation of these devices to existing pump sources and the wavelength flexibility available, external Raman lasers have substantial promise for a diverse range of present and future visible laser applications.

7. External-resonator Raman laser with intracavity SHG/SFG

This section reviews external-resonator Raman lasers that include an intracavity nonlinear crystal for SHG/SFG. The architecture shares the wavelength-selectable (or discretely tunable) characteristic of the intracavity Raman laser devices described in Section 4.2 as well as many of the advantages of the external Raman resonator described in the previous section. As far as we are aware, the architecture has been investigated in detail only in our own group for generating wavelengths in the range 270–325 nm.

7.1. Design characteristics

Fig. 9 shows an example of the basic resonator design. In contrast to simple external-resonator Raman lasers of the previous section, the design includes a larger cavity mirror spacing and curvature to accommodate the nonlinear mixing crystal, and a means is included to efficiently output couple the output harmonic. Output coupling may be achieved in several ways. In this depicted example, the end-mirror M2 was highly reflective at the output frequencies and the second harmonic/sum frequency was output coupled from the resonator using a UV-reflecting dichroic mirror M3 placed between the sum-frequency-mixing crystal and the Raman crystal. This method of output coupling ensures that the generated output harmonic is not incident on the Raman crystal. Though it is feasible to remove M3 and have M2 transmit the output beam, the Raman crystal and its coating need to have low losses also at the output wavelengths. For a KGW Raman crystal and UV output wavelengths <350 nm, the rather poor transmission of KGW precludes this option. A further option would be to orient M3 normal to the beam axis and make M2 highly transmitting at the output wavelengths. The disadvantage of this method is the complexity of the M2 mirror coating, brought about by the simultaneous requirement to reflect the Stokes and transmit the second harmonics.

As in Section 4.2, there are $2n$ possible unique SF or SH wavelengths available (each additional Stokes order provides an additional SH wavelength and a unique wavelength by SF generation with the next lowest order), viz., $\nu_i + \nu_j$, where $0 \leqslant i, j \leqslant n$ for up to n Stokes orders oscillating in the Raman resonator. As discussed below, the number of output

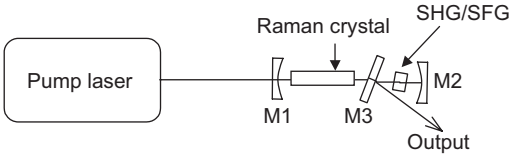

Fig. 9. Experimental arrangement for an external resonator Raman laser with an intracavity nonlinear mixing crystal. M1, input coupler; M2, end mirror and M3, output coupler.

wavelength options expands considerably when using Raman materials that provide high gain on two Raman modes simultaneously.

7.2. Review of experimental results

Table 8 summarises the results of two studies based on a KGW Raman crystal and BBO nonlinear sum-frequency-mixing crystal pumped at 532 nm [100,104]. In the first study, the KGW Raman crystal was oriented to provide maximum gain at the 901 cm^{-1} Raman mode, whereupon up to eight wavelengths were observed in the range 270–320 nm. The output pulse energies were up to 0.22 mJ at 10 Hz pulse repetition rate and average output powers up to 48 mW at 5 kHz [104]. The maximum conversion efficiency was 2.7%, which was achieved for the second harmonic of the first Stokes. As noted in the visible intracavity Raman lasers of Section 4.2, the sum-frequency conversion efficiencies were typically lower than for the second harmonics. This is attributed, at least partially, to the reduced temporal overlap of the subharmonic components in the BBO crystal and the altered dynamics resulting from the competing SRS and SFG depletion processes of the shorter-wavelength Stokes subharmonic. The longest wavelength at 320 nm involved Stokes subharmonics as high as the fourth order. Output at the longer wavelengths was limited by the bandwidth of the resonator mirrors.

In the second and more recent study [100], the wavelength options were investigated for a KGW crystal oriented so that the gain is similar for both 768 cm^{-1} and 901 cm^{-1} Raman modes. It was shown that it was possible to operate simultaneously on two Raman modes (μ_1 and μ_2) and the Stokes wavelengths oscillating in the resonator consisted of not only the multiple orders of both Stokes lines but also combinations of the two Raman modes. To generalize, the possible Stokes output wavelengths combinations are

$$\nu_{ij} = \nu_f - i\mu_1 - j\mu_2$$

where i and j are positive integers and the spectrum included the two separate Stokes spectra (ν_{i0} and ν_{0j}) and mixtures of the two Raman modes (ν_{ij} where i and j are nonzero). Such a "mixing" of the two Raman modes was also noted in the external KGW Raman resonator of Ref. [92] (see also Fig. 7b). It was shown that the maximum number of Stokes wavelengths that can be generated is $\sum_{q=1}^{n_m}(q+1)$ and the number of unique wavelengths available $\sum_{q=0}^{n_m}(4q+1)$, so that the number of harmonic wavelength combinations increases rapidly and the maximum number of Stokes shifts n_m capable of oscillating in the resonator (see Table 9).

For KGW crystal orientations in which the gain was comparable for the 768 and 901 cm^{-1} shifts, up to 14 visible Stokes lines were observed to oscillate in the wavelength range 555–675 nm (corresponding to n_m values up to 5) and up to 30 output wavelengths in the range 271–321 nm by altering the BBO tuning angle. Note that not all wavelengths predicted by Table 9 are observed due to increasing coating losses at longer wavelengths preventing these from reaching the threshold. The conversion efficiency from the input pump energy for each Raman line was typically no higher than 0.5%, which is somewhat lower than that of the single-Raman mode case. The decrease is attributed to the additional loss to Stokes orders not used in generating the output beam or any other subharmonics.

The approach detailed above highlights the significant potential for novel and versatile Raman converters using industry standard pump lasers. The scope to increase the

Table 8
Summary of output wavelengths and performance achieved for 532 nm pumped Raman lasers with intracavity nonlinear mixing

λ_p (nm)	Pump pulse duration FWHM (ns)	Pulse repetition frequency (Hz)	Raman crystal material (Raman mode cm^{-1})	Output wavelength (nm) {assignment}	Max. stokes conversion efficiency (%)	Max. pulse energy (μJ)	Max. output power (mW)	Ref.
532	10	10	KGW (901)	273 $\{\nu_{f+}\nu_1\}$	1.4	104	1.04	[104]
				279 $\{2\nu_1\}$	2.4	223	2.23	
				287 $\{\nu_1+\nu_2\}$	1.1	96	0.96	
				294 $\{2\nu_1\}$	1.6	164	1.64	
				302 $\{\nu_2+\nu_3\}$	1.1	108	1.08	
				311 $\{2\nu_3\}$	1.1	88	0.88	
				320 $\{\nu_3+\nu_4\}$	0.1	7.7	0.08	
532	10	5000	KGW (901)	273 $\{\nu_0+\nu_1\}$	0.85	2.2	11	[104]
				279 $\{2\nu_1\}$	2.7	9.4	47	
				287 $\{\nu_1+\nu_2\}$	0.90	3.4	17	
				294 $\{2\nu_1\}$	1.4	5	25	
				302 $\{\nu_2+\nu_3\}$	0.08	0.3	1.5	
532	10	10	KGW (901, 768)	272 $\{\nu_f+\nu_{10}\}$	–	–	–	[100]
				273 $\{\nu_f+\nu_{01}\}$	–	–	–	
				277 $\{\nu_{10}\times 2\}$[a]	–	–	–	
				278 $\{\nu_{10}+\nu_{01}\}$	–	–	–	
				279 $\{\nu_{01}\times 2\}$	–	–	–	
				283 $\{\nu_{10}+\nu_{20}\}$[a]	0.7	14.2	0.14	
				285 $\{\nu_{01}+\nu_{20}\}$[a]	0.4	12.2	0.12	
				286 $\{\nu_{11}+\nu_{01}\}$	–	–	–	
				287 $\{\nu_{01}+\nu_{02}\}$	–	–	–	
				290 $\{\nu_{20}\times 2\}$[a]	–	–	–	
				291 $\{\nu_{21}+\nu_{01}\}$	–	–	–	
				292 $\{\nu_{11}\times 2\}$[a]	–	–	–	
				293 $\{\nu_{11}+\nu_{02}\}$	–	–	–	
				294 $\{\nu_{02}\times 2\}$	–	–	–	
				296 $\{\nu_{20}+\nu_{30}\}$[a]	–	–	–	
				298 $\{\nu_{30}+\nu_{11}\}$[a]	–	–	–	
				299 $\{\nu_{21}+\nu_{11}\}$[a]	–	–	–	
				300 $\{\nu_{11}+\nu_{12}\}$	–	–	–	
				302 $\{\nu_{02}+\nu_{03}\}$	–	–	–	
				303 $\{\nu_{30}\times 2\}$[a]	–	–	-	
				304 $\{\nu_{21}+\nu_{30}\}$[a]	–	–	–	
				306 $\{\nu_{21}\times 2\}$[a]	–	–	–	
				311 $\{\nu_{03}\times 2\}$	–	–	–	
				310 $\{\nu_{30}+\nu_{40}\}$	–	–	–	
				312 $\{\nu_{21}+\nu_{40}\}$[a]	–	–	–	
				313 $\{\nu_{21}+\nu_{31}\}$	–	–	–	
				318 $\{\nu_{40}\times 2\}$	–	–	–	
				319 $\{\nu_{40}+\nu_{31}\}$	–	–	–	
				320 $\{\nu_{04}+\nu_{03}\}$	–	–	–	
				321 $\{\nu_{31}\times 2\}$				

Note that where several Stokes orders are listed, the output performance corresponds to laser resonator configurations separately optimised for that Stokes order.

[a]Though other assignments were possible, the most likely subharmonics only are listed.

Table 9
Number of Stokes lines and harmonic wavelengths that can be generated as a function of n_m

Max. number of Stokes shifts (n_m)	Stokes lines		Number SFG/SHG wavelengths	
	1 Mode	2 Modes	1 Mode	2 Modes
1	1	2	2	6
2	2	5	4	15
3	3	9	6	28
4	4	14	8	45
5	5	20	10	66

efficiency of these UV Raman lasers is substantial by optimizing the waist sizes, Raman material and its length, and cavity optics. A major factor limiting efficiency is, however, competition between the nonlinear mixing process and further Raman conversion to higher Stokes orders. Conversion efficiency may thus be improved by increasing the nonlinear coupling coefficient for harmonic mixing, which in practice could be achieved for example by paying additional attention to the beam properties (waist sizes in the nonlinear crystals) and the detailed phase-matching requirements in BBO in order to increase the nonlinear output coupling. Cylindrical focusing geometries, widely used to improve conversion efficiency in BBO, may also be applied in this case by the use of anamorphic resonator optics. Power loss by cascading to higher Stokes may also be reduced by introducing resonator losses at the higher Stokes order by, for example, careful selection of coatings. Note, however, that such approaches are most applicable in boosting efficiencies at a specific wavelength. By addressing these issues, conversion efficiencies several times higher than 10% are projected [104].

The wavelength range 270–320 nm is rich in applications in medicine, defence, and bio- and environmental sensing. Though the tuning range demonstrated above is already large, the accessible wavelength range may also be extended to longer wavelengths by using mirrors of increased bandwidth. Other Raman materials may also bring about advantages for targeting specific wavelengths. The architecture is also well suited to other ranges on exchanging the pump laser. An obvious choice is infrared Nd-doped lasers with intracavity SFG to provide a wavelength-switchable laser source spanning the green to red spectral region.

8. Conclusion

In Sections 3–7 above, we have reviewed Raman-laser-based sources in which an extensive range of output wavelengths in the UV and visible has been obtained using a variety of resonator configurations.

Raman-laser-based sources can be tailored to suit a wide range of applications. External-resonator Raman lasers, with the options of intracavity or extracavity frequency doubling, form a convenient and simple module that can be ‘‘added on’’ to many conventional pulsed Nd lasers or frequency-doubled Nd lasers. Consequently the wavelength range of these conventional lasers can be expanded to include wavelengths that are difficult to reach by other means, with further potential for simultaneous operation at several wavelengths or wavelength-selectable output. Diode-pumped

intracavity Raman lasers, with either intracavity or extracavity doubling, tend to be a more efficient approach to generate outputs, primarily at yellow–orange wavelengths, since high intracavity powers can be accessed.

As is clear from the diversity of laser sources reviewed here, Raman lasers can provide output in a wide variety of temporal formats, including pulsed output at high average powers and multi-kHz pulse repetition frequencies or high pulse energies with low prf's. Most significantly, advances in CW operation of crystalline Raman lasers have been made in the past 3 years, which have enabled efficient CW yellow lasers to be demonstrated with efficiencies similar to those for pulsed lasers.

Average output powers as high as 3 W have been reported for a pulsed, intracavity-doubled intracavity Raman laser [65] operating in the yellow, while pulse energies as high as 90 mJ in the yellow have been obtained by extracavity doubling in an external-resonator Raman laser pumped at 1064 nm [51]. While SRS generally tends to be associated with high-power lasers, it is clear from the works reviewed here that intracavity Raman lasers in particular can be engineered to operate efficiently with output powers of only a few milliwatts—both in pulsed [52,64] and in CW modes [81] using diode-pump powers of only a few watts.

There are several aspects of Raman-laser-based sources that have not been widely addressed in this paper, and indeed are not widely addressed in the literature, and these are the spatial, spectral and temporal properties of Raman laser output. Typically the spatial beam quality tends to be good, largely due to the phenomenon of Raman beam cleanup. Spectrally, the Raman linewidths are usually around 0.1 nm. Temporally, Raman-laser-based sources can be engineered for good long-term stability, but on short time scales the output can have significant levels of noise and instability. Pulse to pulse stability (for pulsed lasers) is frequently poor, and for a CW yellow laser [81], the amplitude stability was around 15%, due primarily to longitudinal mode competition effects. There is clearly scope for a comprehensive investigation of the spatial, spectral and temporal properties of Raman-laser-based sources.

Perhaps the aspect of UV and visible Raman-laser-based sources that is most novel and of greatest significance is the capability for wavelength-selectable laser action in the visible and UV. To our knowledge, such a means for wavelength-selectability has not been reported for any conventional laser sources—indeed it is the cascaded nature of the SRS process that makes the approach effective. The capability of choosing several wavelengths from a single laser device is potentially of great value for applications in medicine, biomedicine and remote sensing, where conventionally several (and separate) lasers are used. There is considerable scope for improving the performance of both the UV and visible wavelength-selectable lasers reviewed here, by employing purpose-designed mirrors with broader spectral coverage. In the case of wavelength-selectable UV lasers, much higher efficiencies are anticipated when the resonator is optimised for efficient frequency doubling, thereby preventing unwanted generation of higher Stokes orders.

Many of the papers reviewed here show the great potential for practical, efficient and versatile devices while their performance could be improved considerably by paying attention to resonator design and by using custom-designed resonator mirrors. There is also potential for engineering new Raman laser architectures, e.g. microchip-style devices in which combinations of laser/Raman/doubling crystals are either sandwiched between mirrors or directly coated.

There are clear applications for Raman-laser-based sources operating in the visible in areas such as dermatology, ophthalmology, biomedicine, display, guide stars and remote sensing, and many of the papers reviewed here have targeted those applications. In time, we can anticipate applications for UV wavelengths, e.g. remote sensing, detection of biological agents or explosives, or for biomedical applications such as drug discovery, mass spectrometry and fluorescence imaging.

This paper has been written with the goal of emphasising the diversity of output wavelengths and other performance characteristics using crystalline Raman-laser-based systems. Compared to the other VIS/UV sources as described in Section 1.2, in particular VECSEL-based sources, which are emerging as the go-to technology for multi-watt visible powers, a Raman-laser-based approach offers many attractive features. These include excellent potential for miniaturisation, relative design simplicity based on widely available components (and therefore low cost), flexible geometries for tailoring output properties, high beam quality, potential to scale to multi-watt powers, and a capability for both CW or pulsed operation (note that VECSELs are limited in this regard by low energy storage capacity). Wavelength-selectable output is a unique feature of crystalline Raman laser sources and may become one of the most significant advantages as we look to the future.

References

[1] F.Q. Jia, Q. Zheng, Q.H. Xue, Y.K. Bu, L.S. Qian, Opt. Commun. 259 (2006) 212–215.
[2] A. Agnesi, A. Guandalini, G. Reali, J. Opt. Soc. Am. B Opt. Phys. 19 (2002) 1078–1082.
[3] H. Ogilvy, J.A. Piper, Opt. Express 13 (2005) 9465–9471.
[4] I. Lee, M. Jalali, N. Vanasse, Z. Prezkuta, W.J. Alford, in: Advanced Solid-State Photonics, Optical Society of America, Narra, Japan, 2008 (OSA Technical Digest Series CD).
[5] Y.F. Chen, S.W. Tsai, Opt. Lett. 27 (2002) 397–399.
[6] E. Heumann, S. Bar, K. Rademaker, G. Huber, S. Butterworth, A. Diening, W. Seelert, Appl. Phys. Lett. 88 (2006) 061108.
[7] R. Paschotta, P.R. Barber, A.C. Tropper, D.C. Hanna, J. Opt. Soc. Am. B Opt. Phys. 14 (1997) 1213–1218.
[8] S. Sinha, C. Langrock, M.J.F. Digonnet, M.M. Fejer, R.L. Byer, Opt. Lett. 31 (2006) 347–349.
[9] D. Georgiev, V.P. Gapontsev, A.G. Dronov, M.Y. Vyatkin, A.B. Rulkov, S.V. Popov, J.R. Taylor, Opt. Express 13 (2005) 6772–6776.
[10] A.C. Tropper, H.D. Foreman, A. Garnache, K.G. Wilcox, S.H. Hoogland, J. Phys. D 37 (2004) R75–R85.
[11] J. Chilla, Q.-Z. Shu, H. Zhou, E. Weiss, M. Reed, L. Spinelli, Recent advances in optically pumped semiconductor lasers, in: Proceedings of Solid State Lasers XVI: Technology and Devices, SPIE, 2007.
[12] A. Richter, E. Heumann, E. Osiac, G. Huber, W. Seelert, A. Diening, Opt. Lett. 29 (2004) 2638–2640.
[13] A. Richter, N. Pavel, E. Heumann, G. Huber, D. Parisi, A. Toncelli, M. Tonelli, A. Diening, W. Seelert, Opt. Express 14 (2006) 3282–3287.
[14] E.O. Ammann, Appl. Phys. Lett. 34 (1979) 838–840.
[15] H.M. Pask, Prog. Quantum Electron. 27 (2003) 3–56.
[16] P. Cerny, H. Jelinkova, P.G. Zverev, T.T. Basiev, Prog. Quantum Electron. 28 (2004) 113–143.
[17] T.T. Basiev, R.C. Powell, in: C.E. Webb, J.D.C. Jones (Eds.), Handbook of Laser Technology and Applications, Institute of Physics, UK, 2003.
[18] J.A. Piper, H.M. Pask, IEEE J. Sel. Top. Quantum Electron. 13 (2007) 692–704.
[19] A. Penzkofer, A. Laubereau, W. Kaiser, Prog. Quantum Electron. 6 (1979) 55–140.
[20] R.W. Boyd, Nonlinear Optics, Academic Press, Inc., San Diego, 1992.
[21] P. Cerny, H. Jelinkova, Opt. Lett. 27 (2002) 360–362.
[22] P. Dekker, J.M. Dawes, P.A. Burns, H.M. Pask, J.A. Piper, T. Omatsu, Power scaling of cw diode-pumped Yb:KGW self-Raman laser, in: Proceedings of the Conference on Lasers and Electro-Optics Europe, IEEE, 2003.
[23] A.A. Kaminskii, K. Ueda, H.J. Eichler, Y. Kuwano, H. Kouta, S.N. Bagaev, T.H. Chyba, J.C. Barnes, G.M.A. Gad, T. Murai, J.R. Lu, Opt. Commun. 194 (2001) 201–206.

[24] A.A. Kaminskii, H.J. Eichler, K. Ueda, N.V. Klassen, B.S. Redkin, L.E. Li, J. Findeisen, D. Jaque, J. Garcia-Sole, J. Fernandez, R. Balda, Appl. Opt. 38 (1999) 4533–4547.
[25] P.G. Zverev, A.Y. Karasik, A.A. Sobol, D.S. Chunaev, T.T. Basiev, A.I. Zagumennyi, Y.D. Zavartsev, S.A. Kutovoi, V.V. Osiko, I.A. Shcherbakov, in: Advanced Solid-State Photonics, Optical Society of America, Coeur D'Alene, ID, 2004.
[26] M. Bass, Handbook of Optics, McGraw-Hill, New York, 1995.
[27] W. Wiechmann, S. Kubota, T. Fukui, H. Masuda, Opt. Lett. 18 (1993) 1208–1210.
[28] J.D. Bierlein, H. Vanherzeele, J. Opt. Soc. Am. B Opt. Phys. 6 (1989) 622–633.
[29] T.T. Basiev, A.A. Sobol, P.G. Zverev, V.V. Osiko, R.C. Powell, Comparative spontaneous Raman spectroscopy of crystals for Raman lasers, Appl. Opt. 38 (1999) 594–598.
[30] P.G. Zverev, T.T. Basiev, A.A. Sobol, V.V. Skornyakov, L.I. Ivleva, N.M. Polozkov, V.V. Osiko, Stimulated Raman scattering in alkaline-earth tungstate crystals, Quantum Electron. 30 (2000) 55–59.
[31] J.Y. Wang, H.J. Zhang, Z.P. Wang, W.W. Ge, J.X. Zhang, M.H. Jiang, Growth properties and Raman shift laser in tungstate crystals, J. Cryst. Growth 292 (2006) 377–380.
[32] S.H. Ding, X.Y. Zhang, Q.P. Wang, F.F. Su, S.T. Li, S.Z. Fan, Z.J. Liu, J. Chang, S. Zhang, S.M. Wang, Y.R. Liu, Highly efficient Raman frequency converter with strontium tungstate crystal, IEEE J. Quantum Electron. 42 (2006) 78–84.
[33] M.E. Doroshenko, T.T. Basiev, S.V. Vassiliev, L.I. Ivleva, V.K. Komar, M.B. Kosmyna, H. Jelinkova, J. Sulc, Comparative study of the lasing properties of self-Raman capable Nd^{3+} doped tungstates and molybdates under diode pumping, Opt. Mater. 30 (2007) 54–57.
[34] D. Shuanghong, Z. Xingyu, W. Qingpu, S. Fufang, J. Peng, L. Shutao, F. Shuzhen, C. Jun, Z. Sasa, L. Zhaojun, Theoretical and experimental study on the self-Raman laser with Nd:YVO/sub 4/ crystal, IEEE J. Quantum Electron. 42 (2006) 927–933.
[35] Y.F. Chen, M.L. Ku, L.Y. Tsai, Y.C. Chen, Diode-pumped passively Q-switched picosecond Nd:GD(x)Y(1−x)VO(4) self-stimulated Raman laser, Opt. Lett. 29 (2004) 2279–2281.
[36] A.A. Kaminskii, R.J. Hemley, J. Lai, C.S. Yan, H.K. Mao, V.G. Ralchenko, H.J. Eichler, H. Rhee, High-order stimulated Raman scattering in CVD single crystal diamond, Laser Phys. Lett. 4 (2007) 350–353.
[37] A.A. Kaminskii, V.G. Ralchenko, V.I. Konov, H.J. Eichler, High-order stokes and anti-stokes Raman generation in CVD diamond, Phys. Status Solidi B-Basic Res. 242 (2005) R4–R6.
[38] A.A. Demidovich, A.S. Grabchikov, V. Orlovich, M. Danailov, W. Kiefer, Diode Pumped Diamond Raman Microchip Laser, CLEO, Europe, 2005.
[39] C.C. Davis, Lasers and Electro-Optics: Fundamentals and Engineering, Cambridge University Press, Cambridge, 1996.
[40] V.G. Dmitriev, G.G. Gurzadyan, D.N. Nikogosyan, Handbook of Nonlinear Optical Crystals, Springer, Berlin, 1991.
[41] A.V. Smith, SNLO Nonlinear Optics Code, Sandia National Laboratories, Albuquerque.
[42] Y.F. Chen, Opt. Lett. 30 (2005) 400–402.
[43] J.T. Murray, W.L. Austin, R.C. Powell, in: Advanced Solid State Lasers, Optical Society of America, Coeur D'Alene, ID, 1998.
[44] V.V. Ermolenkov, V.A. Lisinetskii, Y.I. Mishkel', A.S. Grabchikov, A.P. Chaikovskii, V.A. Orlovich, J. Opt. Technol. 72 (2005) 32–36.
[45] A.A. Demidovich, S.V. Voitikov, L.E. Batay, A.S. Grabtchikov, M.B. Danailov, V.A. Lisinetskii, A.N. Kumin, V.A. Orlovich, Opt. Commun. 263 (2006) 52–59.
[46] S.A. Vitsinskii, V.K. Isakov, S.N. Karpukhin, I.L. Lovchii, Sov. J. Quantum Electron. 23 (1993) 1001–1004.
[47] K.S. Johnson, H.M. Pask, M.J. Withford, D.W. Coutts, Opt. Commun. 252 (2005) 132–137.
[48] H.M. Pask, J.A. Piper, Opt. Commun. 148 (1998) 285–288.
[49] J. Findeisen, H.J. Eichler, P. Peuser, Opt. Commun. 181 (2000) 129–133.
[50] J. Findeisen, H.J. Eichler, P. Peuser, A.A. Kaminskii, J. Hulliger, Appl. Phys. B Lasers Opt. 70 (2000) 159–162.
[51] J.T. Murray, W.L. Austin, L.K. Calmes, R.C. Powell, G.J. Quarles, in: Advanced Solid State Lasers, Optical Society of America, Coeur D'Alene, ID, 1997.
[52] W. Baoshan, H. Tan, J. Penga, J. Miaoa, L. Gao, Opt. Commun. 271 (2006) 555–558.
[53] W. Baoshan, T. Huiming, P. Jiying, M. Jieguang, G. Lanlan, Opt. Mater. 29 (2007) 1817–1820.
[54] A. Hamano, S. Pleasants, M. Okida, M. Itoh, T. Yatagai, T. Watanabe, M. Fujii, Y. Iketaki, K. Yamamoto, T. Omatsu, Opt. Commun. 260 (2006) 675–679.

[55] C.B. Rawle, I.T. McKinnie, V.V. Ter-Mikirtychev, W.J. Sandle, in: Advanced Solid State Lasers, Optical Society of America, Coeur D'Alene, ID, 2001.
[56] H.M. Pask, S. Myers, J.A. Piper, J. Richards, T. McKay, Opt. Lett. 28 (2003) 435–437.
[57] R.P. Mildren, H.M. Pask, H. Ogilvy, J.A. Piper, Opt. Lett. 30 (2005) 1500–1502.
[58] S. Li, X. Zhang, Q. Wang, X. Zhang, Z. Cong, H. Zhang, J. Wang, Opt. Lett. 32 (2007) 2951–2953.
[59] G. McConnell, A.I. Ferguson, Opt. Express 13 (2005) 2099–2104.
[60] T. Omatsu, Y. Ojima, H.M. Pask, J.A. Piper, P. Dekker, Opt. Commun. 232 (2004) 327–331.
[61] M. Okida, M. Itoh, T. Yatagai, A. Hamano, T. Omatsu, A compact, all-solid-state, 50 mW Nd^{3+}:$KGd(WO_4)_2$ yellow-orange laser, in: Proceedings of the Conference on Lasers and Electrooptics, IEEE, Piscataway, NJ, USA, 2004.
[62] E.O. Ammann, J. Appl. Phys. 51 (1980) 118–122.
[63] H.M. Pask, J.A. Piper, Opt. Lett. 24 (1999) 1490–1492.
[64] J. Simons, H. Pask, P. Dekker, J. Piper, Opt. Commun. 229 (2004) 305–310.
[65] S. Li, X. Zhang, Q. Wang, Z. Cong, Z. Liu, S. Fan, X. Zhang, J. Phys. D 41 (2008) 055104.
[66] M. Revermann, H.M. Pask, J.L. Blows, T. Omatsu, in: Advanced Solid State Lasers, Optical Society of America, Coeur D'Alene, ID, 2000.
[67] H. Pask, J.L. Blows, J.A. Piper, T. Omatsu, in: Advanced Solid-State Lasers, Optical Society of America, Seattle, WA, 2001.
[68] H.M. Pask, J.A. Piper, IEEE J. Quantum Electron. 36 (2000) 949–955.
[69] H.M. Pask, R.P. Mildren, J.A. Piper, Laser design and energy dynamics in a wavelength-versatile, all-solid-state intracavity cascaded Raman laser, in: Proceedings of the 2005 IEEE LEOS Annual Meeting, 2005, pp. 117–118.
[70] W.S. Otaguro, J. Smith, E. Wienerav, S.P.S. Porto, Phys. Rev. B 6 (1972) 3100.
[71] G.P. Agrawal, Nonlinear Fiber Optics, Academic Press, San Diego, 1995.
[72] J.K. Brasseur, K.S. Repasky, J.L. Carlsten, Opt. Lett. 23 (1998) 367–369.
[73] H.S. Rong, R. Jones, A.S. Liu, O. Cohen, D. Hak, A. Fang, M. Paniccia, Nature 433 (2005) 725–728.
[74] A.S. Grabtchikov, V.A. Lisinetskii, V.A. Orlovich, M. Schmitt, R. Maksimenka, W. Kiefer, Opt. Lett. 29 (2004) 2524–2526.
[75] A.A. Demidovich, A.S. Grabtchikov, V.A. Lisinetskii, V.N. Burakevich, V.A. Orlovich, W. Kiefer, Opt. Lett. 30 (2005) 1701–1703.
[76] H.M. Pask, Opt. Lett. 30 (2005) 2454–2456.
[77] V.N. Burakevich, V.A. Lisinetskii, A.S. Grabtchikov, A.A. Demidovich, V.A. Orlovich, V.N. Matrosov, Diode-pumped continuous-wave Nd:YVO_4 laser with self-frequency Raman conversion, Appl. Phys. B Lasers Opt. 86 (2007) 511–514.
[78] D.J. Spence, P. Dekker, H. Pask, IEEE J. Sel. Top. Quantum Electron. 13 (2007) 756–763.
[79] P. Dekker, H.M. Pask, J.A. Piper, Opt. Lett. 32 (2007) 1114–1116.
[80] P. Dekker, H.M. Pask, D.J. Spence, J.A. Piper, Opt. Express 15 (2007) 7038–7046.
[81] A.J. Lee, H.M. Pask, T. Omatsu, P. Dekker, J.A. Piper, Appl. Phys. B Lasers Opt. 88 (2007) 539–544.
[82] T. Omatsu, H.M. Pask, J.A. Piper, in: Advanced Solid-State Photonics, The Optical Society of America, Narra, Japan, 2008.
[83] R.P. Mildren, H.M. Pask, J.A. Piper, in: Advanced Solid-State Photonics, Optical Society of America, Incline Village, NV, USA, 2006.
[84] P. Apanasevich, V. Lisinetskii, A. Kananovich, A. Grabtchikov, V. Orlovich, M. Schmitt, S. Schlueker, B. Kuestner, W. Kiefer, K. Ichino, A.A. Demidovich, M. Danailov, G. Krylov, Continuous-wave solid-state Raman lasers generating at first and second Stokes wavelengths, in: Proceedings of the European Conference on Lasers and Electro-Optics, Optical Society of America, Munich, Germany, 2007.
[85] S.N. Karpukhin, A.I. Stepanov, Sov. J. Quantum Electron. 16 (1986) 1027–1031.
[86] C. He, T.H. Chyba, Opt. Commun. 135 (1997) 273–278.
[87] W.T. Roberts Jr., J.T. Murray, W.L. Austin, R.C. Powell, J.R.P. Angel, in: Adaptive Optical System Technologies, SPIE, 1998.
[88] D.W. Coutts, Personal communication, 2002.
[89] A.A. Kaminskii, C.L. McCray, H.R. Lee, S.W. Lee, D.A. Temple, T.H. Chyba, W.D. Marsh, J.C. Barnes, A.N. Annanenkov, V.D. Legun, H.J. Eichler, G.M.A. Gad, K. Ueda, Opt. Commun. 183 (2000) 277–287.
[90] P. Zverev, T.T. Basiev, I.V. Ermakov, W. Gellerman, in: Advanced Solid-State Lasers, Optical Society of America, Seattle, USA, 2001.
[91] R.P. Mildren, Unpublished work, 2004.

[92] R.P. Mildren, M. Convery, H.M. Pask, J.A. Piper, T. McKay, Opt. Express 12 (2004) 785–790.
[93] A.I. Vodchits, D.N. Busko, V.A. Orlovich, V.A. Lisinetskii, A.S. Grabtchikov, P.A. Apanasevich, W. Kiefer, H.J. Eichler, P.Y. Turpin, Opt. Commun. 272 (2007) 467–475.
[94] V.A. Lisinetskii, A.S. Grabtchikov, P.A. Apanasevich, M. Schmitt, B. Kuschner, S. Schlucker, V.A. Orlovich, J. Raman Spectrosc. 37 (2006) 421–428.
[95] J.T. Murray, R.C. Powell, T. Roberts, C. Shelton, R. Angel, D. Sandler, Sodium guide star laser for the 6.5 m MMT telescope, in: Proceedings of the ESO Workshop on Laser Technology for Laser Guide Star Adaptive Optics Astronomy, European Southern Observatory, Germany, 1997.
[96] W.T. Roberts Jr., Guide star lasers for adaptive optics, Thesis, University of Arizona, Arizona, 2002.
[97] H. Injeyan, E.C. Cheung, J.G. Ho, Patent, US5796761, 1998.
[98] P.G. Zverev, M.E. Doroshenko, T.T. Basiev, Raman laser for sodium-layer laser-guide-star experiment, in: Conference Digest of the 2000 Conference on Lasers and Electro-Optics Europe, 2000, Cat. no. 00TH8505, vol. 1, p. 1.
[99] P.G. Zverev, T.T. Basiev, M.E. Doroshenko, V.V. Osiko, in: Advanced Solid State Lasers, Optical Society of America, Davos, Switzerland, 2000.
[100] R.P. Mildren, J.A. Piper, Opt. Express 16 (2008) 3261–3272.
[101] S.H. Ding, X.Y. Zhang, Q.P. Wang, F.F. Su, S.T. Li, S.Z. Fan, Z.J. Liu, J. Chang, S.S. Zhang, S.M. Wang, Y.R. Liu, Opt. Express 13 (2005) 10120–10128.
[102] D.D. Smith, Noncollinearly pumped solid state Raman laser, Patent, US6556339, 2003.
[103] R.L. Byer, Solid state system for frequency conversion using Raman-active media and non-linear media, Patent, US5673281, 1997.
[104] R.P. Mildren, H. Ogilvy, J.A. Piper, Opt. Lett. 32 (2007) 814–816.